Argelander-
Institut
für
Astronomie

UNIVERSITÄT BONN

Non-Accreting Helium Stars as Progenitors of Thermonuclear Supernovae

Masterarbeit zur Erlangung des akademischen Grades

"Master of Science (M.Sc.)"

im Studiengang Astrophysik

Angefertigt von

Savvas Chanlaridis

am

Argelander-Institut für Astronomie

Vorgelegt der

Mathematisch-Naturwissenschalftlichen Fakultät
der
Rheinische Friedrich-Wilhelms-Universität Bonn
Deutschland

October, 2019

I hereby declare that this thesis was formulated by myself and that no sources or tools other than those cited were used.

Date	Signature

1. Gutachter: Prof. Dr. Norbert Langer
2. Gutachter: Prof. Dr. Michael Kramer

To my Loved Ones

τί δὴ τοῦτό ἐστι Πυθαγόρας ἐρωτώμενος,
ʽτὸ θεάσασθαιʼ εἶπε ʽτὸν οὐρανόνʼ

When Pythagoras was asked [about the purpose
for which humans were created], he said,
"To look upon the heavens"

ABSTRACT

Thermonuclear explosions of white dwarfs are being observed as Supernovae-Ia. The progenitors, and the exploding mechanism of such phenomena are topics with a lot of room for debate, although the scientific consensus is that these systems originate from binaries in which mass transfer, or coallesence of the binary triggers a runaway process in the deep interior of the white dwarfs leading to a catastrophic explosion without any remnants.

Since SNe-Ia exhibit significant variations in terms of their spectra, is is rather unclear if the companion star is a non-degenerate star (single degenerate scenario, SD), or another white dwarf (double degenerate scenario, DD), or even some combination of scenarios. In this thesis, we performed numerical caluclations exploiting the MESA stellar evolution code in order to examine single, non-rotating Helium stars as potential progenitors of SNe-Ia. By adopting various values for the metallicity environment, and by allowing efficient overshooting mixing, we found that He-stars in the mass range $1.8 - 2.7$ $M_{\odot}$ develop a degenerate ONe core, that retains a small amount of carbon. Subsequent shell burning can force the degenerate ONe core to grow to near-Chandrasekhar mass, igniting the residual carbon and destabilizing the star, ultimately resulting in a thermonuclear explosion.

In the absence of an extended accretion phase, these models can provide an alternative channel within the SD scenario, which can have a non-negligible effect on the observational rates of SNe-Ia.

x

ACKNOWLEDGMENTS

During my effort for the completion of this Master Thesis many people had stand by me and contributed in one way or another.

CONTENTS

LIST OF FIGURES

LIST OF TABLES

Chapter 1

INTRODUCTION

The cycle of life and death of stars baffled astronomers for many years. The study of stellar structure and evolution continues -up to this date- to be of paramount importance, since it is crucial to our understanding of various branches of astronomy, e.g. the structure of galaxies, and chemical history of the Universe.

The aim of this thesis is to investigate and get an insight in one of the most debated topics in Stellar Astrophysics; the connection between the progenitor and remnant masses, especially in the case of double neutron star binary systems. The existence of those systems was recently confirmed by the detection of gravitational waves emitted during a merging event, accompanied by the detection of a kilonova -the "afterglow" of such an event- as described in the seminal paper of the LIGO/VIRGO collaborations (Abbott et al. 2017).

In this chapter, a synopsis that extends from the formation to the death of helium stars will be attempted. A detailed coverage of the principles of stellar evolution is beyond the scope of this thesis and a fundamental knowledge is assumed. Moreover, for the interested reader, there are classical textbooks (Kippenhahn et al. 2012; Clayton 1968; Prialnik 2000; Eggleton 2006) covering almost every aspect in the field of stellar astrophysics. Nevertheless, for the sake of completeness, a small introduction to several fundamental notions, tailored to our needs, will also be carried out in the next few pages.

1.1 Helium stars

From the large primordial molecular clouds, protostars are being constantly formed via a process called *gravoturbulent cloud fragmentation*. When the accretion of the surrounding material from the protostellar core ceases, the protostar is said to be in the *pre-main sequence* (PMS) phase of its evolution, and continues to contract under the force of gravity until the central temperature becomes sufficiently high for nuclear fusion reactions on hydrogen to occur. At this point, the star enters the *main sequence* (MS) evolutionary phase as a zero-age main sequence (ZAMS) star where it will spend most of its life.

During the MS stage, the star converts hydrogen to helium either via the pp-chain reactions, or via the CNO cycles, depending on its initial mass and chemical composition. Slowly but steadily, the hydrogen in the core is being consumed by the aforementioned nuclear networks, and helium builds up forming a helium core. This process continues until the hydrogen in the stellar core is depleted, resulting to an inert hydrogen envelope engulfing the newly formed He-core; subsequently, the star exits the MS phase and the nuclear reactions in its interior that provided the necessary pressure support against gravity, effectively stop. Since the star is not in an equilibrium state anymore, it starts to contract until hydrogen is ignited in a shell around the inert helium core. At this point, the star enters the so-called

red-giant branch (RGB) and the hydrogen-rich envelope, on top of the H-burning shell, inflates rapidly whilst the He-core continues to contract due to the *mirror principle* (see Kippenhahn et al. 2012, p. 369).

As we will explain in a moment, the hydrogen envelope can be lost when the star is in the RGB phase, with more than one ways, exposing the He-core of the star. This naked, hydrogen deficient, He-core is what we refer to as a *helium star*. We can classify He-stars into two groups: low-mass *hot subdwarfs* (sd) that can be further subdivided into several categories (e.g. sdB, sdO) based on their spectra, and more massive *Wolf-Rayet* (WR) stars that can also be subdivided into several classes (e.g. WN, WC). For a more detailed discussion we refer the reader to the work of Han et al. (2002); Han et al. (2003); Heber (2009); Chiosi & Maeder (1986); Langer (2012).

1.1.1 Formation of helium stars

Helium stars can be formed either in isolation or as part of a binary system. In both scenarios, the physical mechanism that is responsible for the stripping of the hydrogen envelope is of the utmost importance.

In the former case of a single He-star, the necessary mass loss is being achieved due to strong, radiation-driven, stellar winds. However, the specifics of such a process have not been fully resolved yet, and an enhanced mass loss scheme, e.g. caused by rotational mixing, magnetic fields, or even strong He-flashes should be considered for the progenitor of the He-star (Sweigart 1997; Heber 2009).

In the case where the He-star progenitor is part of a binary system, the required strong mass loss can be achieved via different channels, depending on how wide the binary system is. These channels include the stable Roche-lobe overflow (RLO) and the Common Envelope (CE) ejection. We will discuss these mass loss mechanisms below. It should be mentioned that sdB stars can also originate from the merging of two helium white dwarfs (He-WD) in a close binary, resulting to an object with enough mass to ignite helium (Han et al. 2002).

1.1.2 Evolution of single helium stars

Once the He-star progenitor has been stripped from its hydrogen envelope during the RGB phase, the compression of the core continues until it reaches the necessary conditions for helium to ignite at its centre. The ignition of core helium burning signifies the transition to the helium main sequence (He-MS) as a He-ZAMS star. The last two concepts are defined in a similar way to the (hydrogen) main sequence and ZAMS respectively.

During the He-MS stage, the star burns its ^{4}He supply via the triple-alpha process producing carbon (^{12}C) and the stable oxygen isotope ^{16}O, as a byproduct. When the helium in the core is depleted, the contraction/expansion process we described above is repeated; the idle metal core that has been formed, consists mainly of carbon, oxygen, neon, and magnesium and it is surrounded by a He-rich envelope. This whole structure will contract until helium is ignited in a shell at the bottom of the envelope, followed by the ignition of carbon in the centre (given that the star is massive enough). The fate of the He-star at this point depends on its mass; if it has not retain enough mass for carbon ignition, it will gradually cool off and end its life as a carbon-oxygen white dwarf (CO WD). On the other hand, if it is massive enough to ignite carbon, either on or off centre, its fate could be an oxygen-neon-magnesium white dwarf (ONeMg WD), a hybrid white dwarf (CONeMg WD), or even collapse as a supernova.

To demonstrate the aforementioned stages, the evolutionary track of a 3.0 $M_\odot$ He-star (with and without mass loss) is illustrated in the $T_c - \rho_c$ plane (Fig 1.1) (see also Habets 1986a,b; Nomoto 1987). The letters denote the beginning and end of several phases up to the off-centre neon ignition. The A-B phase shows the contraction that follows after the RGB stage of the progenitor. The moment of core He-ignition is denoted by the black circle at point B, and marks the entrance to the He-MS phase (B-C). At point C, helium has been exhausted and the core contracts whilst He-shell burning follows. During the D-E phase, the carbon is ignited in the core making a loop in the diagram around $\rho_c = 10^6$ g cm^{-3}.

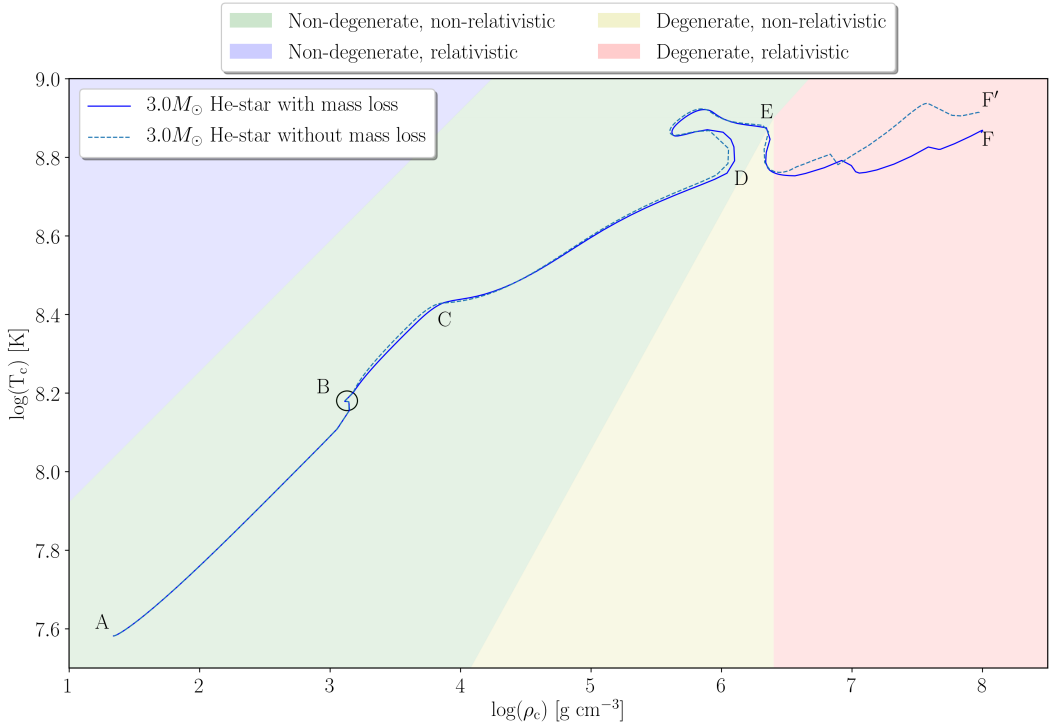

Figure 1.1: The evolution of a 3.0 $M_\odot$ He-star, with and without mass loss. The point where the star enters the He-MS as a He-ZAMS can be seen as a small hook inside the black circle. An analytic explanation of the letters along the evolutionary tracks, is provided in the text. The coloured areas illustrate the different regimes of pressure.

Finally, the E-F/F′ shows the carbon-shell burning along the contraction of the O-Ne-Mg core; at the endpoint (F/F′), neon is ignited off-centre.

Conveniently, in the same figure one can see the approximate regimes of pressure which are illustrated as coloured regions. For the conditions in the green area, the stellar material is non-degenerate and non-relativistic hence the dominant pressure can be approximated by the ideal gas law ($P_{\rm gas}$). The blue area shows the region where the gas is still in a non-degenerate state but the temperature is so high that forces the electrons to move with speeds that are comparable to the speed of light. Under these conditions, the pressure provided by the exerted radiation ($P_{\rm rad}$) begins to dominate over the gas pressure. Moving to higher densities the electron gas becomes degenerate, first non-relativistically (yellow area) and then relativistically (red area). In both cases the pressure is provided by the degenerate electron gas. From the diagram it becomes clear that degeneracy can be lifted if the temperature is sufficiently high.

These boundaries for the pressure regimes can be easily found if we equate the relevant expressions of pressure given by the equation of states for each regime (e.g. $P_{\rm gas} = P_{\rm rad}$, for the two non-degenerate regions). In reality the transition among the different regimes is continuous and not sharp as depicted here, which can be misleading. Nevertheless, this way of imaging provides us with a visual aid of when in the evolutionary stage of a star relativistic, or quantum mechanical effects can be of great importance.

For a more complete and comprehensive overview of the evolution of single He-stars, we provide, in the form of a Kippenhahn diagram, the net energy production rate with respect to the internal structure of the 3.0 $M_\odot$ star (with mass loss) we used in the example above (Fig 1.2). In this diagram, the x-axis expresses the remaining time of the calculations whilst the y-axis shows the inner structure of the star in terms of mass coordinates. The color scale is associated with the energy production. By taking a careful look, we observe that during He-burning in the convective core, the star experiences an approximately ~ 0.3 $M_\odot$ mass loss via stellar winds. As a result of this core burning process, a C-core of ~ 1.2 $M_\odot$ is

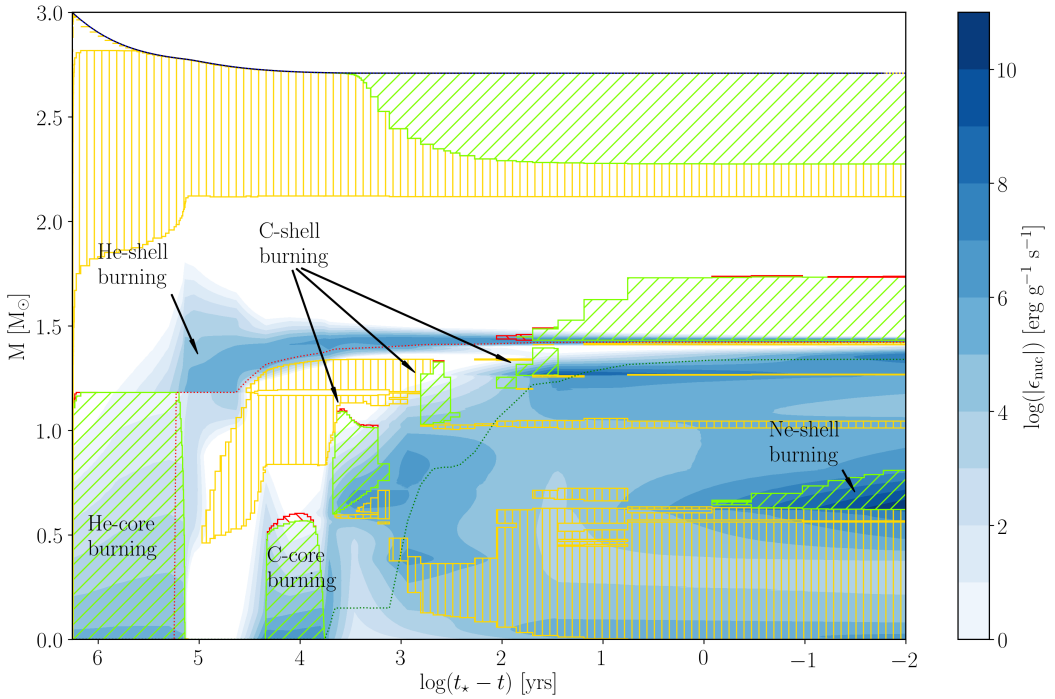

Figure 1.2: Kippenhahn diagramm for a 3.0 $M_\odot$ He-star with mass loss. The green and gold hatched areas denote convective and thermohaline mixing respectively. Red solid lines represent areas with semi-convective mixing. The black, red, and green dotted lines show the build-up of helium, carbon, and oxygen core mass respectively.

formed that continues to grow up to ~ 1.42 $M_\odot$ due to He-shell burning. Similarly, an oxygen core is formed of about ~ 1.34 $M_\odot$ as a result of the more advanced burning stages.

Mixing mechanisms

Although protostars begin their life with, a more or less, uniform elemental composition which is the same as the composition of the cloud they originated from, the ongoing nuclear reactions transform and create new elements that are not necessarily distributed uniformly throughout the stellar interior. This is because there are several ways for a star to stir and mix its material. These mixing mechanisms are usually caused by various instabilities and can contribute on different levels based on specific conditions. In this section we will briefly explain four major mixing processes leaving the effects of rotation for later discussion.

Maybe the most effective way to transfer material is with *convection*. Thermal variations across different shells of the star will lead to density variations and, consequently, to buoyancy driven flows of the fluid. Essentially, what this means is that a hot parcel of fluid will rise due to buoyancy forces and a colder parcel will sink. This process is very efficient for transporting more heavy elements produced in the deep interior of the star towards the surface via bulk motions (dredge-up) and vice versa. The stability of a layer against convection is given by the *Ledoux* criterion

$$\nabla_{\rm rad} < \nabla_{\rm ad} - \frac{\phi}{\delta}\nabla_\mu \tag{1.1}$$

which, in the case of chemically homogeneous layers ($\nabla_\mu = 0$), reduces to the *Schwartzschild* criterion

$$\nabla_{\rm rad} < \nabla_{\rm ad} \tag{1.2}$$

where $\nabla_{\rm rad}$ is the radiative temperature gradient describing the logaritmic temperature variation with depth (for the case that energy is transported by radiation); $\nabla_{\rm ad}$ is the adiabatic temperature gradient defined similarly to $\nabla_{\rm rad}$ but for the case of adiabatic compression or expansion; and the second term of the equation accounts for changes in chemical composition. For a detailed explanation of the symbols and the implications of those criteria, see (Kippenhahn et al. 2012, pp. 49-51).

The composition gradient in the Ledoux criterion acts as a stabilizing agent in weakly, thermally unstable regions leading to a slower mixing rate. These zones are not mixed by convection but rather by another process, called *semi-convection* (see Spruit 2013; Langer et al. 1983; Langer 1991).

Another mechanism that has an important consequence in stellar evolution, is *convective overshooting*. During this phenomenon, a parcel of fluid carried away by convection will overshoot beyond the boundary of the unstable region and into the stable region. This is caused by the inertia of the convective material and thus, it travels some distance further than the region in which it was accelerated until it loses all of its momentum. For this reason, convective overshooting introduces a large uncertainty in the extent of mixed regions (see Saslaw & Schwarzschild 1965; Stothers & Chin 1990; Roxburgh 1998, for a detailed discussion on the effects of overshooting).

The fourth major mixing process is called *thermohaline* mixing. It occurs when the molecular weight decreases with depth, e.g. a helium layer on top of a hydrogen-rich layer due to accretion in a binary system. The heavier elements will eventually sink in whilst the lighter material will rise, re-establishing the mean molecular weight to being larger as we move towards the centre of the star[1]. However, thermohaline mixing is believed to play a lesser role in the evolution of single stars and becomes important in accreting binaries (see also Cantiello, M. & Langer, N. 2010; Charbonnel, C. & Zahn, J.P. 2007).

Effects of rotation

The evolution of stars can be significantly altered if they are rotating. This is true for most -if not all- stars found in nature, since they inherit angular momentum during the collapse of the already turbulent molecular cloud they originated from. Rotation can influence the shape of stars, their lifetimes since the centrifugal force lowers the internal pressure that is necessary to balance gravity, and their abundance profiles. The latter is a result of several rotation-induced instabilities like the Eddington-Sweet circulation, the dynamical shear instability, and the secular shear instability, to name a few. Especially the Eddington-Sweet circulation and the shear instability play an important role to the transportation of angular momentum between different layers of the star.

The importance of rotational mixing is difficult to be overstated. As an example, we mention the results of Maeder (1987) who found that, for massive stars, a bifurcation of the evolutionary tracks in the Hertzprung-Russel diagram appears around a critical rotation. This is caused by the inability of the composition gradient (∇_μ) to prevent turbulent diffusion above this critical rotation, thus the diffusive mixing leads to an almost chemically homogeneous evolution, i.e. the star exhibits the same composition everywhere. These homogeneous models are likely to result to the formation of WR stars before the end of their hydrogen-burning phase, which increases the WR lifetime, and potentially lead to the formation of gamma-ray bursts in low-metallicity environments (Yoon & Langer 2005).

A detailed coverage of the effects of rotation in stellar evolution is offered by Langer et al. (1997); Heger et al. (2000); Hirschi et al. (2004); Maeder et al. (2006); Langer (2012); Palacios (2013). More on the rotation-driven transportation of angular momentum and associated mechanisms can be found in Heger et al. (2005); Langer (2012) as well as in the work of Spruit (2002) where a discussion on the importance of dynamo-generated magnetic fields takes place.

[1] This is a slow process since gravitational settling can be balanced by a supporting temperature gradient that could lead to the formation of doubly diffusive instabilities (e.g. salt-fingers).

Stellar winds and mass loss

It has been long since we first discovered that stars experience a continuous outflow of material from their surface causing them to gradually lose a significant fraction of their initial mass. This ejection of material is called *stellar wind* and several mechanisms trying to explain its origin have been proposed over the years.

Stellar winds do not affect all stars in the same way; it depends on the mass of the star and its current evolutionary stage. Low-mass stars that are in the MS phase, like our Sun, are hardly influenced from the generated winds. However, more massive and post-MS stars experience strong, usually radiation accelerated[2], winds that peel off large quantities of mass, and changing this way their surface chemical composition. The mass loss rates and the terminal velocities of these winds appear to vary significantly with luminosity, temperature, metallicity, and other global stellar parameters such as the radius (Hamann et al. 1982; de Jager et al. 1988; Nugis & Lamers 2000; Yoon 2017).

Observations of spectral features have allowed us to establish several empirical relations and constraints for the mass loss rates; especially in the case of WR stars which are known for their strong optically thick winds, the mass loss rates have been revised downwards by almost an order of magnitude (Nugis & Lamers 2000) compared to earlier estimations (Hamann et al. 1995; Langer 1989) due to the influence of clumping and the asymmetrical structure of the winds. The prescription of Nugis & Lamers (2000) is currently the most popular for the mass loss rate of WR stars, although Yoon (2017) raises a word of caution and argues that in the aforementioned prescription, the considered metallicity dependence is not related to the initial metallicity, but rather to the self-enrichment of carbon and oxygen at the surface due to mass loss.

Finally, it should be mentioned that in the case of rotating stars, stellar winds will also carry away some of the specific angular momentum of the star along with the ejecta material. Additionally, magnetic fields coupled to the wind plasma in a co-rotation, will slow down the spin of the star which, in turn, will affect the mass loss rate and the angular momentum losses of the system. This is known as *magnetic braking* and plays an important role in stellar evolution, especially in the case of binary systems (see Ivanova & Taam 2003). For a complete review of our current understanding of stellar winds see Lamers & Cassinelli (1999); Smith (2014).

1.2 Evolution of binary systems

So far we have concerned ourselves with the evolution of single He-stars. However, the majority of stars are formed in binary systems, being gravitationally bound to each other, and exhibiting a variety of orbital periods that can range from minutes to millions of years. If the two stars are well separated, then the interaction between them should be minimal and both stars will evolve essentially as if they were isolated. Nevertheless, in the case of a close binary, strong interactions might initiate mass transfer from one star to another, altering significantly their structure, how they evolve, and subsequently, their final fate.

In the next few pages, an attempt to briefly explain the basic concepts that govern any interacting binary system will be made. At the end, we will comment on the formation of double neutron star (DNS) binaries which is of particular interest for the aim of this thesis. For a more detailed coverage of the evolution of binary systems we refer to Ivanova (2015); Podsiadlowski (2014); Postnov & Yungelson (2014); Eggleton (2006); Tauris & van den Heuvel (2006).

[2]These winds can be driven either by radiation pressure on dust condensations that have been formed in the upper atmosphere of stars, or by radiaton pressure on the resonance absorption lines of metals such as carbon and nitrogen.

1.2.1 Interaction and orbital parameters

In any multiple star system, the gravitational fields of all interacting components influence the motion of the whole system which is governed by the, well known, Newton's laws of motion. This is dubbed as *n-body problem* and is one of the most notoriously difficult problems in physics since it exhibits a chaotic behaviour with no general analytical solution; for this reason, a numerical approach is required.

In the case of a binary system, the n-body problem is reduced to the *restricted three-body problem* with the effective gravitational potential

$$\Phi = -G\left(\frac{M_1}{r_1} + \frac{M_2}{r_2}\right) - \frac{1}{2}\Omega^2 r_3^2 \tag{1.3}$$

where r_1, r_2 are the distances to the center of the stars M_1 and M_2 respectively; Ω is the orbital angular velocity; and r_3 is the distance to the rotational axis of the binary (Tauris & van den Heuvel 2006, p. 639). If we require the cumulative forces acting on a test mass, m, to vanish

$$\boldsymbol{F}_t = -m\nabla\Phi = 0 \tag{1.4}$$

then eq (1.3) yields five stationary solutions where the gravitational force cancels out the centrifugal force caused by the relative motion of the two stars around each other. The points where eq (1.4) holds true, are called *Lagrangian points* or *libration points*, L_n, $n = 1, 2, 3, 4, 5$. Hence, if a test mass was to be positioned in any of those five equilibrium points, it would maintain its position relative to the two stars. More information on the stability of Lagrangian points, in the sense of what would happen if one applied a small perturbation on a test mass sitting in a libration point, can be found in Szebehely (1967); Celletti & Giorgilli (1990); Schwarz et al. (2012).

From the five Lagrangian points, the L_1 plays a key role in the evolution of binary systems since the equipotential surface[3] passing through that inner point, defines the *Roche-lobe*. The shape of the equipotential surfaces is illustrated in Fig 1.2; they assume a concentric spherical shape in proximity to the two stars whilst, as a result of the combined gravitational influence of the two masses, they get distorted when we move further away.

During the various evolutionary stages, the star might inflate and increase its radius to such a degree that the volume of the star exceeds the volume defined by its Roche-lobe. This will cause a transfer of surface material from that star to its companion via the L_1 point triggered by the unbalanced pressure in that direction; this process is known as *Roche-lobe overflow* (RLOF) and the donor star can lose a substantial amount of its total mass. Unfortunatelly, there is no analytical expression for the size of a Roche-lobe in a given binary. However, Eggleton (1983) has proposed a numerical approximation of the radius of the Roche-lobe given by the following equation

$$\frac{R_L}{\alpha} = \frac{0.49q^{2/3}}{0.6q^{2/3} + \ln(1 + q^{1/3})} \tag{1.5}$$

where α is the orbital separation, and $q \equiv M_{\text{donor}}/M_{\text{accretor}}$ is the mass ratio of the binary components. These are the two most important orbital parameters that we need to know in order to follow the evolution of the binary.

It is maybe worth mentioning that as matter spills across the inner Lagrangian point, it forms an *accretion disk* rather than falling directly onto the companion star. This happens simply because the accreted material possesses the same angular momentum as the donor star, and unless there are non-conservative processes able to remove some of the angular momentum of the accreted gas, it will continue to orbit around the companion star.

[3] An equipotential surface is defined as the collection of all points in the system that share the same value of the effective gravitational potential, Φ.

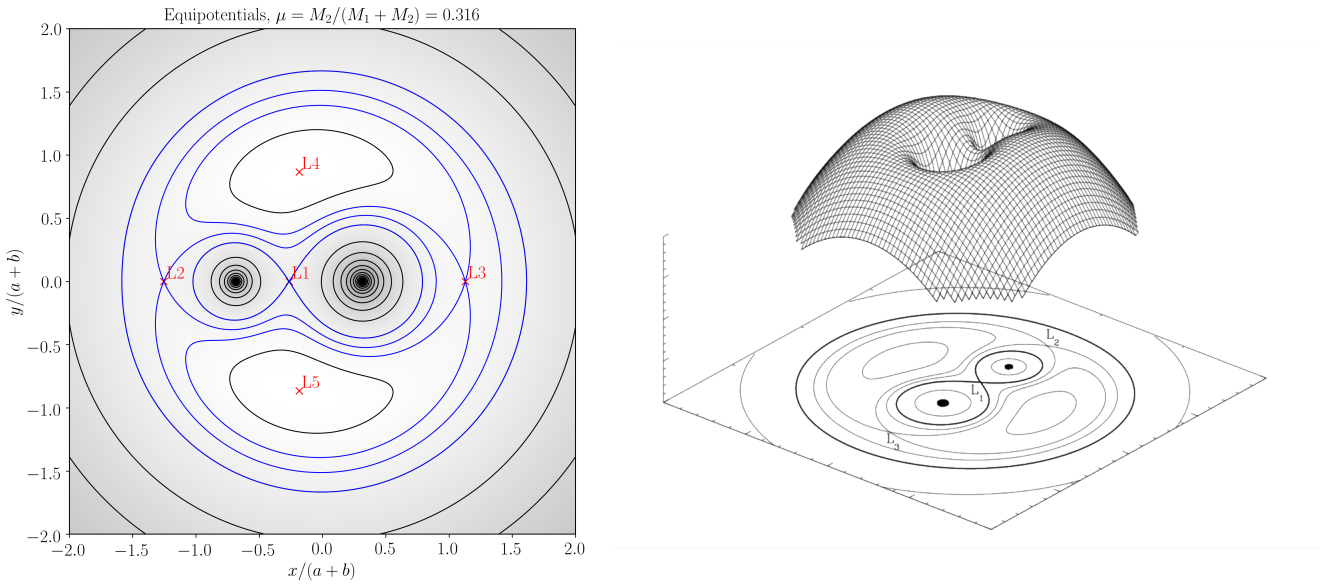

Figure 1.3: **Left panel**: Equipotential lines in the x-y orbital plane of a rotating binary with a reduced mass ratio of $\mu = 0.316$. In this setup, M_1 is the more massive and is located at $x = +a$, whilst M_2 is the less massive and is at $x = -b$. The inner equipotential surface that passes from the L_1 Lagrangian point, defines the "teardrop"-shaped Roche-lobes, one for each star. Contour lines passing through the Lagrange points are marked with blue colour. The image was created based on a `python` script, courtesy of Zingale (2016). **Right Panel**: 3D representation of equipotential surfaces. The image was adapted from van der Sluijs (2006).

Based on which equipotential surfaces are filled, we can classify binary systems into three categories (see also Weigert 1968): (i) *detached binaries* where the radii of both stars are much smaller than their orbital separation; neither of the two stars fills its respective Roche-lobe, and they evolve almost independently of each other, (ii) *semi-detached binaries* where only one of the two stars fills its Roche-lobe leading to distortion of the equipotential surfaces from their spherical shape, and mass transfer occurs, and (iii) *contact binaries* where both stars fill their Roche-lobe. This situation results to a shared, common atmosphere that might be ejected, stripping the system from a significant amount of mass.

1.2.2 Mass transfer

From the discussion above, it becomes clear that the mass transfer rate via RLOF and its stability depends on the extent to which the donor star overfills its Roche-lobe. Especially the stability of the mass transfer depends on how the donor star responses to this sudden mass loss; for *stable* mass transfer, the donor must remain within its Roche-lobe (see Ivanova 2015; Postnov & Yungelson 2014; Soberman et al. 1997; Kalogera & Webbink 1996, for discussion).

Based on the evolutionary status of the donor star when it fills its Roche-lobe, we can discern three cases of mass transfer (Kippenhahn & Weigert 1967; Lauterborn 1970):

(i) *Case A*: mass transfer commences while the star is still in the MS, i.e. during core hydrogen burning;

(ii) *Case B*: the donor star fills its Roche-lobe after the Hygrogen has been depleted from its core but before helium ignition;

(iii) *Case C*: refers to RLOF after the exhaustion of helium in the core, and includes all the subsequent stages.

For helium stars in particular, we can define the cases *BA*, *BB*, and *BC* for mass transfer during He core burning, He-shell burning, and carbon core burning respectively.

Finally, if the donor star is massive enough, it is likely to experience very strong stellar winds that will remove a considerable amount of mass even without filling its Roche-lobe. A fraction of this mass lost via winds might be accreted by its companion star; this is refered to as *wind mass transfer*, and although it provides a less efficient way to transfer mass, compared to RLOF, it can be important in some binaries.

1.2.3 Common envelope

When mass is transfered via RLOF in a dynamically unstable manner, i.e. when the convective envelope of the donor star continues to expand despite the mass loss, the mass loss rate naturally increases. The companion star accretes material stably at its thermal timescale, which is orders of magnitude larger than the dynamical timescale at which the donor star loses mass, thus it grows until it fills its Roche-lobe as well (Izzard et al. 2012); at this point, the two stars form a contact binary system, and share a common envelope (CE).

Since the orbital plane of the two stars lies within the CE, a drag force will be developed due to friction, caused by the motion of the stars. The system then goes through a *spiral-in* phase, during which a dissipation of orbital angular momentum leads to the decay of the orbit (i.e., a reduction of the orbital separation). This plunge phase occurs on an orbital timescale of a few years (Izzard et al. 2012), and the energy lost from the orbit is being deposited in the surrounding envelope. The reaction of the envelope to this energy deposition is to expand and potentially ejected from the binary. The ultimate outcome of the CE stage is a more tight binary with a reduced total mass (assuming that the orbital shrinkage during the CE phase didn't result to a merging of the two cores). For this reason, although the physical background of the CE phase described above is still not well understood, it has been hypothized that it plays a crucial role in the formation of a wide variety of binary systems, including double neutron star systems. For a complete review of our current understanding of CE evolution, we refer to the work of Ivanova et al. (2013).

1.2.4 Angular momentum losses

Orbital angular momentum variations, and the mechanisms via which this can occur play an important role in the evolution of a binary since it directly affects the orbital period of the system. Angular momentum can be extracted from a binary system on different timescales (Yakut et al. 2008) mainly via the following processes:

(i) *Non-conservative mass transfer*: If during mass transfer, the companion star accretes only a fraction of the mass lost from the donor, the rest will carry away some of the specific angular momentum.

(ii) *Magnetic braking*: As it was mentioned above, the differential rotation of stars is responsible for the production of magnetic fields and, subsequently, magnetized stellar winds. Interactions with the magnetic fields can give raise to tidal effects, causing a rotating star to sync and corotate with the orbit (tidally locked system). If the spin of the star is originally larger than the orbital period, this is essentially translated to angular momentum removal from the binary (see also Rappaport et al. 1983).

(iii) *Gravitational waves*: These are perturbations of the space-time manifold caused by various kinds of motion and asymmetric distribution of masses in a close binary. Like classical waves, gravitational

waves carry energy (often dubbed as gravitational radiation) that is being lost from the system causing the angular momentum to decrease and the orbit to shrink (see also Peters 1964; Riles 2013).

1.2.5 Double neutron star systems

Since the aim of this thesis is to investigate the connection between progenitor and remnant masses in double neutron star (DNS) binaries, it is considered appropriate to devote a subsection on the formation and the importance of these incredible systems.

Initially massive binaries which their components are close enough to interact with each other, will undergo several stages that are plagued with uncertainties before they end up as neutron stars. The most acceptable scenario for the formation of DNS systems up to this day begins with the evolution of the more massive (primary) component, which naturally happens on a shorter timescale than its companion. The primary star will fill its Roche-lobe transferring material to the companion star and exposing its helium core. Further evolution of the newly formed He-star will lead to a supernova explosion which could unbound the whole system.

If the binary survives the explosion, the first-born neutron star can be detected as a radio pulsar orbiting a massive main sequence star (OB-star). As the latter evolves, mass transfer will be initiated and the system can be observed as a high-mass X-ray binary (HMXB) due to the accelerated infalling material onto the surface of the neutron star. When the secondary star expands to a degree that can engulf the neutron star, a common envelope is formed; assuming that during the spiral-in phase a coalescence of the two stars will not occur, a binary system consisting of a neutron star and a helium star will emerge.

Depending on the mass of the He-star, its evolutionary stage, and the orbital separation of the two components, a second mass transfer event may occur stripping the donor star from its helium-rich envelope and spinning up the accreting neutron star. The neutron star that has been spun up during this process is often dubbed *recycled* and is believed to be the origin of millisecond pulsars.

Finally, the second neutron star will be formed in a low-energy supernova (see below). The final fate of such systems, depending on the post-SN orbital separation and eccentricity of the binary, is to merge due to gravitational waves damping. The remnant -if any- that is left behind from such an event is most likely a single black hole. All the stages leading to the formation of DNS binaries that were described above are presented in Fig 1.3 and exhaustively discussed in the work of Tauris et al. (2017).

Double neutron star binaries are remarkable systems and excellent sources of gravitational waves. This enables them to act as probes and shed some light on all the uncertain evolutionary stages that lead to their formation, e.g. CE evolution, nature and asymmetries of SNe explosions, velocity kicks imparted onto newborn neutron stars as well as their mass distribution. For a more complete coverage see (Tauris et al. 2017; Ivanova et al. 2003; Dewi & Pols 2003, and references therein).

1.3 Stellar transients

Transient stars are defined as objects which experience a strong variation in their brightness, that can be observed within a human lifetime, due to various instabilities ranging from magnetic-powered flares in small, dim red dwarfs (M-dwarfs) to thermonuclear shell/core flashes, and gravitational collapse of iron cores. Transients can be non-periodic and/or non-recurring events depending on the nature of the underlying instability. Generally, unstable processes like magnetic reconnection, accretion instabilities, and shell flashes have a tendency not to disrupt the star so they might occur a number of times during the lifetime of the star. On the other hand, known disruptions include supernovae and merging events. Here we will briefly discuss the latter scenario of explosive transients.

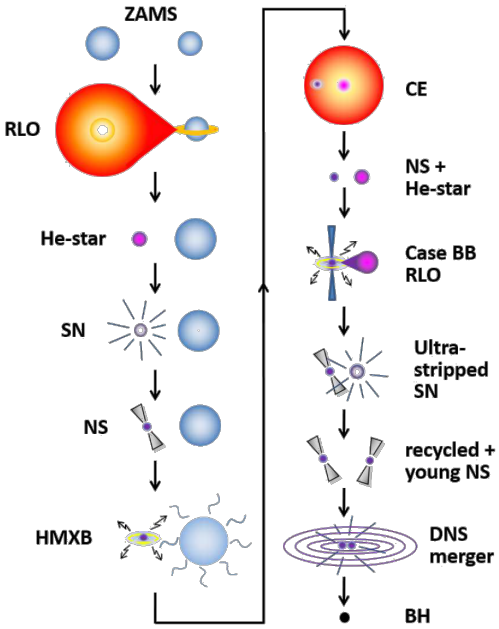

Figure 1.4: Illustration of the formation of a DNS system which merges within a Hubble time and produces a single black hole. Image and caption taken from Tauris et al. (2017).

1.3.1 Types of Supernovae

Massive stars will end their short lives in an extremely luminous supernova (SN) explosion leaving behind a compact object which is either a neutron star or a black hole, depending on the initial mass of the progenitor star, and enriching their host galaxy with all the elements they forged during their lifetime. Classification of supernovae has been traditionally done by their observational characteristics like spectral features, and properties of their light curves as seen in Fig 1.4 (see Filippenko 1997; Turatto 2003).

Whilst there are many physical mechanisms that could potentially lead to a supernova, the connection between the progenitor of the explosion and the type of supernova we eventually observe is still unclear. However, we can differentiate between core collapse SNe (CCSNe) where pressure support is being removed from the core of the star via numerous processes, and thermonuclear explosions of mass-accreting white dwarfs. We will not discuss here the latter case, the associated exploding mechanisms, or how it is related to the type-Ia but the interested reader can refer to the work of Hillebrandt & Niemeyer (2000); Wang (2018); Branch & Wheeler (2017).

For the case of a star that experiences a gravitational core collapse, there are several channels via which pressure support could be removed from the core; next, we discuss a few aspects of these channels and -to a certain degree- the underlying exploding mechanism.

Iron core collapse SNe (Fe-CCSNe)

During the final stages of evolution, if the star is massive enough it will develop an inert iron core. As temperature increases in the core, the energy of the photons becomes sufficiently high to start photo-disintegration on the ^{56}Fe nuclei. This process removes pressure from the core, forcing it to contract until electrons and protons fuse together in a process called *neutronization*. As in all weak interactions, neutronization is accompanied by the production of neutrinos that do not contribute to the pressure support against gravity since they escape the star much faster than photons, and effectively acts as a cooling mechanism carrying energy away. Depending on the mass of the core, the degeneracy pressure provided by the neutrons might be sufficient to cease the collapse leading to the formation of a neutron

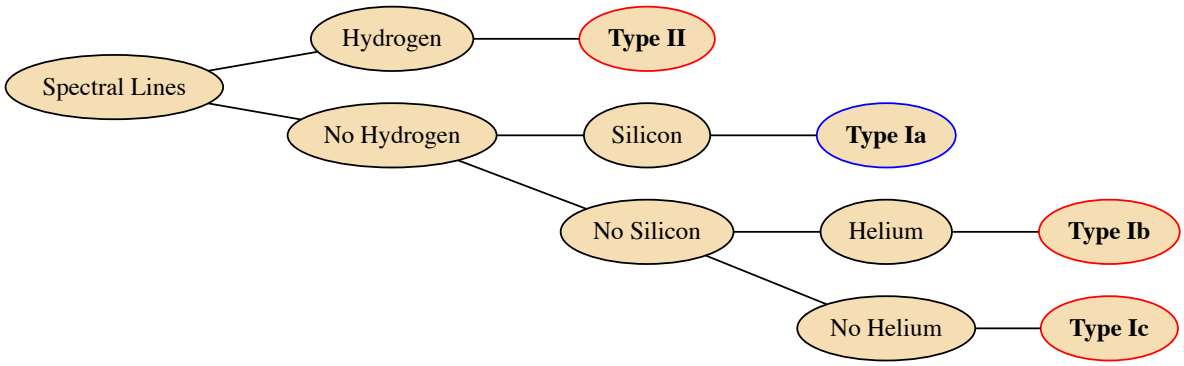

Figure 1.5: Basic classification of supernovae based on their spectra lines. Further sub-groups can be identified if we take into consideration the behavior of their light curves. Type Ia (here marked with a blue circle) is associated with thermonuclear runaway reactions rather than core collapse (red circles).

star.

Following Müller et al. (2016), the infalling material will bounce on the surface of the neutron star sending back a shock wave that quickly stalls due to photodisintegration of heavy nuclei and neutrino losses; this is the *pre-explosion phase* and it becomes clear that another energy source is needed in order to have a successful explosion. This source is believed to be a (gain) region behind of the shock where energy deposition of neutrinos leads to heating. The shock revival occurs once the accreted material spends sufficient time in the gain region to receive enough energy from neutrinos to negate its binding energy; the shock is re-energized by the radiation and expands outwards again. At this point we have entered the *explosion phase*. In the case of a very massive core, degeneracy pressure from neutrons is not enough to balance the gravitational pressure, therefore the star will continue to collapse forming a stellar mass black hole. More on the progenitors of CCSNe and relevant exploding mechanisms can be found in Smartt (2009); Couch (2017).

Electron capture SNe (ECSNe)

Formation of an iron core is not the only way to remove pressure support. Less massive stars will form a degenerate ONeMg core where the pressure is provided by the degenerate electrons. If the degenerate core reaches a critical mass of $M_{\rm crit}^{\rm EC} = 1.37$ M$_\odot$ (Nomoto 1984), electron captures on ^{24}Mg and ^{20}Ne nuclei will reduce the number of electrons, and thus the pressure against gravitational contraction, triggering the collapse of the core. The energy released from the electron captures will eventually lead to an oxygen deflagration[4]. However, since oxygen is ignited in a highly degenerate environment there will be no expansion as a response to the temperature increase, as in the case of non-degenerate matter; instead, this increase of temperature will accelerate the rate of fusion and, consequently, the temperature will again increase in a runaway process. The contraction of the core, due to loss of pressure support, increases the density and leads to more rapid electron captures, at a rate that can overcome the oxygen deflagration and continue to collapse up to neutron star density.

The core is believed to collapse more rapidly than in the case of Fe-CCSNe, launching a shock wave in accordance with core bounce and subsequent neutrino heating as explained above. The final result is a dim supernova with a relatively low explosion energy and low ^{56}Ni ejecta mass (Jones et al. 2016).

[4]A deflagration process refers to a subsonic front that propagates via thermal conduction as opposed to a detonation process where a supersonic burning front is driven by shock waves.

Two-dimensional simulations have shown that the explosion exhibit almost spherical symmetry (Nomoto et al. 2014) since the rapid nature of the explosion leave less time for asymmetries to develop (Jones et al. 2016), thus ECSNe do not impart large natal velocity kicks to the newly-formed neutron star.

The late evolutionary stages of these lower-mass stars are riddled with uncertainties resulting to a very narrow mass-range for the progenitors of ECSNe. To complicate things even more, if these stars are part of a binary system, interactions between the two stars can give raise to new channels for ECSNe to emerge. For this case, we refer to Siess, L. & Lebreuilly, U. (2018); Giacobbo & Mapelli (2018); Poelarends et al. (2017).

Pair instability SNe (PISNe)

So far we discussed the final fate of massive stars that develop an iron core, and the less certain evolution of lower-mass stars that develop a degenerate ONeMg core. At the opposite end we find the case of very massive stars, i.e. stars with initial mass $M_{\rm init} > 100$ M$_\odot$. It has been suggested (Langer 2012) that these enormous stars undergo a dynamical collapse before core oxygen ignition, caused by electron-positron pair creation that effectively reduces the radiation pressure in the stellar core, leaving behind no remnant. PISNe are expected to produce a wide variety of SN types depending on their mass range (Gilmer et al. 2017). We will not discuss further this particular branch of SNe since it poses no interest for this thesis. For this reason, the inquisitive reader is referred to the work of Langer et al. (2007); Woosley (2017); Kozyreva et al. (2017); Gilmer et al. (2017).

1.3.2 Type Ib/c Supernovae

Supernova explosions of naked helium stars are expected to be observed as Type Ib or Type Ic due to their lack of a hydrogen mantle (Fig 1.4). Additionally, in order to be classified as Type Ic, the progenitor star must be also stripped from its helium envelope[5] either via strong stellar winds or binary interactions. As Yoon et al. (2010) mention, population studies indicate that the majority of SNe Ib/c are produced in binary systems without the need of single star progenitors in order to match their observed rate. This can be important since the nature of the explosion will determine if the binary shall remain bound after the explosion or break apart into two loose components.

Of particular interest for this thesis is the case of *ultra-stripped* SNe as described in Tauris et al. (2015, 2013). The authors showed that a helium star can be heavily stripped as a result of the binary interaction with a neutron star, ultimately leading to a very faint SN-Ic with a mass ejecta of only $\lesssim 0.2$ M$_\odot$. The implication of such small amount of ejecta can be quite important in the formation of DNS systems since the binding energy of the envelopes is expected to be smaller than the one found in normal SNe, imparting only a small kick in the second neutron star.

For an overview of the expected light curve properties of ultra-stripped SNe, see Moriya et al. (2017).

1.4 Thesis Outline

In this thesis, we performed numerical calculations with the MESA stellar evolution code in order to construct a detailed grid of helium stars in the mass range $1.5 \leq M/M_\odot \leq 3.5$, and study their viability as supernovae progenitors. The results of our calculations are presented in the following chapters which are organized as follows; In chapter 2, we examine/discuss blah blah. In chapter 3, the detailed grid of single helium stars is presented blah blah. Chapter 4 addresses the question of how the evolution is

[5] There is a caveat in this formulation; helium can be detected only if it has been excited by the radioactive decay of ^{56}Ni. If a substantial amount of He is present after the explosion but -somehow- shielded from ^{56}Ni, the SN would be still classified (falsely) as Type Ic! The amount of synthesized ^{56}Ni along with the efficiently mixing into the He-envelope remains crucial for that matter.

altered when these helium stars are part of a binary configuration. Finally, in chapter 5 we summarize the key results of this thesis and we discuss possible future work.

Chapter 2

METHODS

For the puproses of this thesis we performed numerical calculations using the one dimensional, stellar evolution code **M**odules for **E**xperiments in **S**tellar **A**strophysics (`MESA`) (Paxton et al. 2011, 2013, 2015, 2018). In this section, we present the very basic aspects of `MESA` and the physical assumptions we used in our attempt to model the evolution of single and binary stellar systems.

2.1 Modules for Experiments in Stellar Astrophysics

`MESA` is an open-source stellar evolution code which provides a modular approach to stellar modelling. Each of the available modules is responsible for the delivery of a specific aspect of the required physics (e.g. microphysics modules provide necessary equations of state and nuclear networks, utilization of macrophysics modules to treat mixing processes etc) in order to succesfully construct a computational stellar model.

For a spherically symmetric star in hydrostatic equilibrium the structure of the star is governed by the following four differential equations, in Lagrangian form

$$\text{Mass conservation:} \qquad \frac{\partial r}{\partial m} = \frac{1}{4\pi r^2 \rho} \tag{2.1}$$

$$\text{Hydrostatic equilibrium:} \qquad \frac{\partial P}{\partial m} = -\frac{Gm}{4\pi r^4} \tag{2.2}$$

$$\text{Energy conservation:} \qquad \frac{\partial l}{\partial m} = \epsilon - \epsilon_\nu + \epsilon_g \tag{2.3}$$

$$\text{Energy transport:} \qquad \frac{\partial T}{\partial m} = -\frac{T}{P}\frac{Gm}{4\pi r^4}\nabla = \frac{T}{P}\frac{\partial P}{\partial m}\nabla \tag{2.4}$$

and its evolution by the composition equations (eq. 2.5)

$$\frac{\partial X_i}{\partial t} = \frac{m_i}{\rho}\left(\sum_j r_{ji} - \sum_k r_{ik}\right), \qquad \mathrm{i} = 1, \ldots, \mathrm{n} \tag{2.5}$$

where X_i is the mass fraction of all relevant nuclei $i = 1, \ldots, n$ with mass m_i (Kippenhahn et al. 2012, p. 89).

MESA is able to simultaneously solve the coupled structure and composition equations without the need of operator splitting, where we alternately solve the spatial (structure) and temporal (evolution) equations. This is achieved by exploiting a generalized Newton-Raphson iterative solution which is most commonly referred to as the *Henyey method* (Wilson 1981; Kippenhahn et al. 2012, p. 106); a grid of finite mesh points has to be set up, essentially dividing the structure into a large number of discrete mass cells where the differential equations need to be calculated. Assuming appropriate boundary conditions, a trial solution has to be guessed in advance which will be later improved after a number of consecutive iterations, and until the required degree of accuracy has been reached in order for the code to converge on a final solution. If after a specified number of iterations the model fails to converge, MESA will retry the calculation using a smaller timestep; this process will be repeated until the code finds an acceptable model to converge or until it reaches a limit in the timestep reduction.

Finally, during the star's evolution, MESA will automatically adjust the mesh and redistribute it based on the structure and composition profiles of the model at the beginning of each timestep. For a proper insight into timestep selection and mesh refinement see Paxton et al. (2011).

Chapter 3

RESULTS

In this chapter we present the results blah blah

3.1 Type-Ia Supernovae from non-accreting progenitors

In this section, we present a novel progenitor channel for Supernovae-Ia along with a first-order approximation concerning the formation frequency of the corresponding progenitor systems, energetics of the explosion, and nucleosynthetic signature.

DRAFT VERSION SEPTEMBER 3, 2019
Typeset using LaTeX **twocolumn** style in AASTeX62

TYPE Ia SUPERNOVAE FROM NON-ACCRETING PROGENITORS

JOHN ANTONIADIS,[1,2] SAVVAS CHANLARIDIS,[2] GÖTZ GRÄFENER,[2] AND NORBERT LANGER[2,1]

[1]*Max-Planck Institut für Radioastronomie, Auf dem Hügel 69, 53121, Bonn DE*
[2]*Argelander Institut für Astronomie, Auf dem Hügel 71, 53121, Bonn DE*

Submitted to ApJ *Letters*

ABSTRACT

Type Ia supernovae (SNe Ia) are manifestations of helium-deficient stars disrupting in a thermonuclear runaway. While explosions of carbon-oxygen white dwarfs are thought to account for the majority of events, part of the observed diversity may be due to varied progenitor channels. We demonstrate that helium stars with masses between 1.8 and 2.5 $\mathrm{M}_\odot$ may evolve into highly degenerate, near-Chandrasekhar mass cores with helium-deficient envelopes, that subsequently ignite carbon and oxygen explosively at densities $\sim 10^{9.26-9.77}$ gr cm^{-3}. This happens either due to compression from shell burning (when the core has a hybrid CO/NeO composition), or following inigition of residual carbon triggered by exothermic electron captures on ^{24}Mg (for a NeOMg-dominated composition). We argue that the resulting thermonuclear runaways are likely to prevent core collapse, leading to the complete disruption of the star in a SN Ia explosion with a kinetic energy of $\sim 10^{51}$ erg. The frequency of progenitor systems would suffice to account for a large fraction of SNe Ia in star-forming galaxies.

Keywords: binaries: general - stars: evolution - supernovae: general

1. INTRODUCTION

Despite their central role in Astrophysics and Cosmology, the origin and physics of Type Ia supernovae (SNe Ia) remain uncertain (Maoz et al. 2014). Typical SN Ia luminosities ($\sim 10^{43}\,\mathrm{erg\,s^{-1}}$) and ejecta velocities ($\sim 10^{4}\,\mathrm{km\,s^{-1}}$), require ^{56}Ni masses and kinetic energies of order $\sim 0.6\,\mathrm{M}_\odot$ and $\sim 10^{51}\,\mathrm{erg}$ respectively. These properties suggest that SNe Ia are most likely stars that disrupt in thermonuclear explosions, rather than core-collapse events. Carbon/oxygen white dwarfs (CO WDs) approaching the Chandrasekhar-mass limit ($M_{\rm Ch}$) are the most promising progenitor systems, as they can produce explosions broadly consistent with observations (Nomoto 1982; Churazov et al. 2014).

Conventional stellar evolution channels, produce stable CO WDs with masses below $\sim 1.0\,\mathrm{M}_\odot$. Consequently, matter accretion onto the WD is required to trigger an explosion, either via stable transfer from a donor star (single-degenerate channels; SD), or in a merger event (double-degenerate channels; DD). Thus far, all of the proposed SD or DD variants encounter substantial difficulties in providing a self-consistent model for SNe Ia (Livio & Mazzali 2018). For instance, SD channels require considerable fine-tuning of the mass accretion rate for the WD to grow in mass. In addition, the interaction between the SN blast and the donor star or the circumbinary material, is expected to produce signatures which are rarely or never seen, e.g. some contribution to the SN luminosity at early times (Kasen 2010), radio synchrotron emission (Harris et al. 2016), and Hα lines due to unburned hydrogen. DD mergers on the other hand may produce a variety of outcomes, ranging from prompt explosions to long-lived remnants, or the delayed formation of a neutron star (Livio & Mazzali 2018). In addition, their overall contribution to the observed SN Ia rate may be too low (van Kerkwijk et al. 2010; Claeys et al. 2014a; Sato et al. 2015).

Over the past 50 years, systematic studies of SN Ia explosions have revealed a large diversity in their properties (Taubenberger 2017). Examples of extreme outliers include luminous (e.g. SN 1991T; Filippenko et al. 1992) and ultra-luminous (e.g. SNLS-03D3bb; Howell et al. 2006) SNe, SN 1991bg-like transients which are faint and rapidly evolving (Ruiz-Lapuente et al. 1993), and SN 2012ca-like events, dubbed SNe Ia-CSM, in which there is evidence for interaction with a dense circum-stellar medium (Bochenek et al. 2018). Even among "normal" SNe Ia there is appreciable scatter in rise times, maximum luminosities, ejecta velocities and spectral evolution (Livio & Mazzali 2018). Finally, there seems to be a correlation with environment, as active galaxies typically host more, and brighter SNe Ia (Maoz et al. 2014).

While part of this diversity can be understood within the framework of SD and DD families, there may exist additional evolutionary pathways leading to SNe Ia. Here, we explore

Corresponding author: John Antoniadis
janton@mpifr.de

an alternative channel in which a thermonuclear runaway leading to a SN Ia can be initiated during the late evolution of a degenerate core of neon-oxygen (NeO) or carbon-neon-oxygen (CNeO) composition that approaches $M_{\rm Ch}$. Such progenitors are generally thought to produce massive WDs or electron capture supernovae (ECSN) (e.g., Nomoto & Kondo 1991; Gutierrez et al. 1996; Takahashi et al. 2013). Here however, we show that near-$M_{\rm Ch}$ (C)NeO cores originating from intermediate mass helium stars ($\sim 1.8-2.5\,{\rm M}_\odot$) —a common product of binary interactions— can ignite their residual carbon and oxygen explosively at densities $\lesssim 10^{9.77}\,{\rm gr\,cm^{-3}}$, before the onset of ^{20}Ne(e$^-$,ν_e)^{20}Fe electron capture reactions (Section 2). In addition, the envelope is promptly lost via winds or due to binary interactions, leaving behind a helium-free structure. We demonstrate that the combination of final composition and available energy, would yield explosions with luminosities and ejecta velocities consistent with classical SNe Ia (Section 2.4). This mechanism does not require accretion from the binary companion and therefore may contribute significantly to the SN Ia rate in young stellar populations (Section 3).

2. (C)NeO CORES: FORMATION AND EVOLUTION

Highy degenerate stellar cores of neon-oxygen composition form inside stars with ZAMS masses between 7 and $11\,{\rm M}_\odot$ (Farmer et al. 2015; Woosley 2019). After core helium burning, such stars enter a super-asymptotic giant branch (SAGB) phase, characterized by a dense CO core and an extended hydrogen envelope. As the core becomes increasingly more degenerate, it cools substantially due thermal neutrino emission. An important consequence is that the critical temperature for ^{12}C ignition is first attained off-center, creating a convectively bound flame that propagates inwards (Siess 2006).

Carbon burning in SAGB stars is affected by complex mixing processes due to a combination of inverse composition gradients, overshooting, semi-convection and rotation. The penetration of NeONaMg ashes into unburned regions, may impact significantly the propagation of the burning front. Mixing generally reduces the thermonuclear reaction rate, leaving behind substantial amounts of residual carbon. In extreme cases, the flame can be quenched completely, resulting in a hybrid structure, with a CO core, surrounded by a NeO mantle (Denissenkov et al. 2013).

The subsequent evolution and final fate of the star depend critical on the competition between neutrino cooling due to the presence of ^{23}Na^{23}Ne and ^{25}Mg^{25}Na Urca pairs, and compressional heating due to accretion from the helium burning shell (Schwab et al. 2017). SAGB stars are subject to significant dredge-up and thermally unstable shell burning. These effects may impact substantially the ability of the core to grown in mass fast enough.

However, thermal pulses and dredge-up episodes do not occur when the hydrogen envelope is lost, e.g. due to a common envelope (CE) event in a binary system (Woosley 2019). In such a case, helium shell burning is stable, allowing the core to approach the Chandrasekhar mass limit. In what follows, we build detailed numerical models to investigate the combined effects of residual unburned ^{12}C, Urca cooling and constant mass accretion from shell burning, in the late evolution of (C)NeO cores that originate from helium stars.

2.1. *Numerical Calculations: Input Physics*

We use MESA version 10386 to follow the evolution of two helium-star models, M1 and M2, with masses of 2.4 and $1.8\,{\rm M}_\odot$ respectively. The initial models have uniform compositions with $Y = 0.98$ and $Z = 0.02$ (solar abundances are taken from Grevesse & Sauval 1998). We employ a nuclear network that considers 43 isotopes, from ^{1}H to ^{58}Ni. Reaction rates are based on the `JINA reaclib v2.0` compilation (Cyburt et al. 2010). Electron screening factors and cooling rates from thermal neutrinos are evaluated as in Farmer et al. (2015), and references therein. Weak interaction rates are taken from Suzuki et al. (2016). Wind mass loss rates are calculated using MESA's `Dutch` compilation (Paxton et al. 2013).

Our baseline convection model considers standard, thermohaline and semiconvectional mixing. Convective stability is evaluated using the Ledoux criterion. By default, MESA uses standard mixing-length theory (MTL; Cox & Giuli 1968) for convective mixing and energy transport. However, following carbon burning, both our models develop dynamically-unstable super-Eddington envelopes, causing numerical difficulties. For this reason, we decided to employ the "enhanced" MLT option available in MESA (Paxton et al. 2013), which artificially reduces the super-adiabatic gradient leading to an enhanced convective energy transport efficiency. This allows us to follow the evolution of the core after carbon burning without interruptions.We further discuss this choice and its impact on the envelope evolution and the final mass in Section 4. The MLT mixing length parameter is set to $a_{\rm MLT} = 2.0$ for both models. For thermohaline and semi-convection we employ the Kippenhahn et al. (1980) and Langer et al. (1983) treatments respectively. In addition to the baseline mixing parameters, in M2, we also consider the effects of overshooting, adopting an efficiency of $f_{\rm ov} = 0.014$ across all convective boundaries, including the base of the carbon-burning flame. While mixing at this interface may not occur in reality, we use this as a means to quench the flame before reaching the center. Other mixing processes such as rotation and thermohaline can lead to the same outcome for similar initial helium core masses (Farmer et al. 2015). The MESA inlists are publicly available[1]. A more extended grid which explores a broad range of initial masses, metallicities and overshooting parameters will be presented in an accompanying paper (Chanlaridis et al. 2019).

2.2. *Simulation results*

Figure 1 shows Kippenhahn diagrams for M1 and M2, focusing on the evolution after central helium depletion. M1

[1] http://cococubed.asu.edu/mesa_market/inlists.html

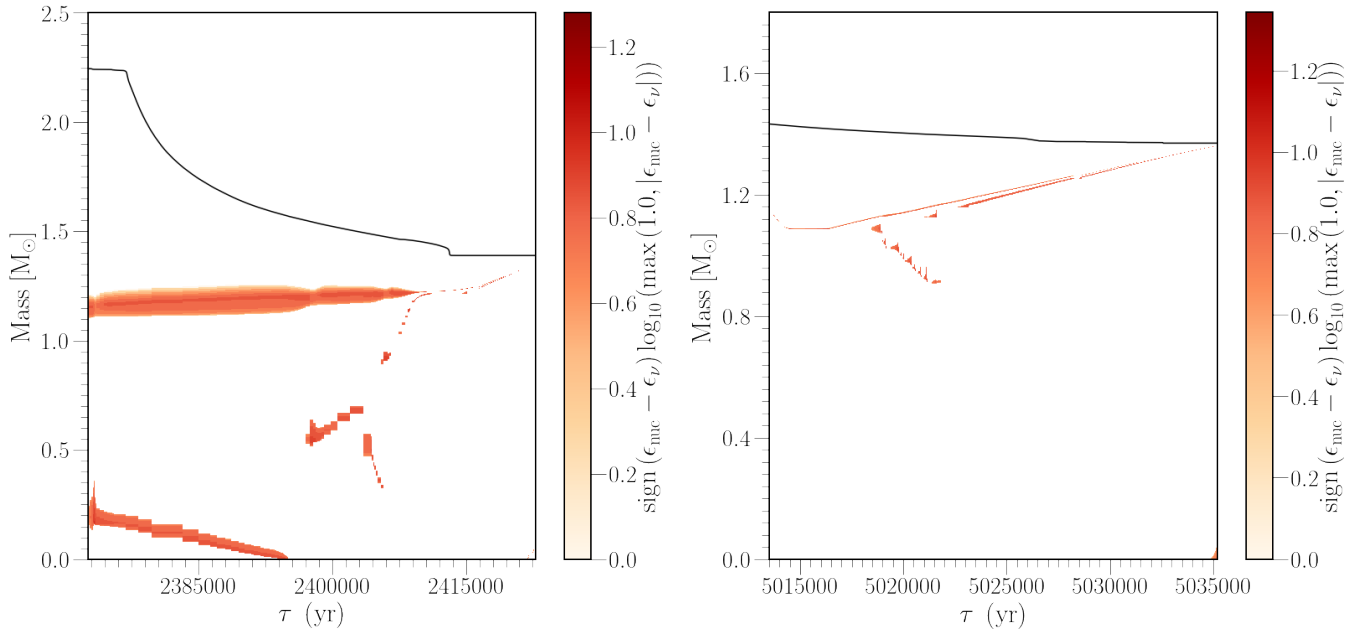

Figure 1. Kippenhahn diagrams following the evolution of M1 (left) and M2 after core helium depletion. Colored areas indicate regions in which nuclear burning occurs, i.e. locations for which the nuclear energy $\epsilon_{\rm nuc}$ exceeds energy losses due to neutrion emission, ϵ_ν.

first ignites carbon at mass coordinate $\sim 0.3\,{\rm M}_\odot$, when the total mass is $2.25\,{\rm M}_\odot$ and the CO core has a mass of $\sim 1.15\,{\rm M}_\odot$. The initial flame is followed by secondary flashes which propagate in both directions. Some of these episodes seem to occur only after a small critical mass of carbon has been accumulated below the burning shell. The entire carbon-burning phase lasts for about 40,000 yr. During most of this time, the star is a red giant with a low-density convective envelope ($R \simeq 125\,{\rm R}_\odot$, $\log_{10}(T_{\rm eff}/{\rm K}) \simeq 3.75$, $\log_{10}(L/\,{\rm L}_\odot) \simeq 4.3$), and loses mass at a rate of $\dot{M} \simeq 10^{-6}\,{\rm M}_\odot\,{\rm yr}^{-1}$, in good agreement with recent KEPLER models (Woosley 2019).

As the core contracts and its surface gravity increases, the surrounding burning shells become progressively thinner. The envelope responds by expanding and the stellar structure resembles closely that of an SAGB star. The last $\sim 5,000$ yr of the evolution are characterized by rigorous burning in two neighbouring shells which eventually merge, resulting in a ^{20}Ne flash. In this phase the star reaches extremely high luminosities up to $\log L/L_\odot = 6.25$ resulting in a strong stellar wind that lasts for ∼1000 yr and eventually removes the He-rich envelope.

The evolution of the envelope during the final stages depends critically on the energy transport mechanism above Eddington lumonisities. With the enhanced MLT option employed in our calculations, M1 briefly becomes a yellow supergiant as the envelope expands to $R \simeq 900\,{\rm R}_\odot$ while remaining dynamically stable. The strong wind of $\dot{M} \simeq 10^{-3.8}\,{\rm M}_\odot\,{\rm yr}^{-1}$ in this phase is in the same range as theoretically expected maximum values for super-Eddington winds (Owocki et al. 2004; Smith & Owocki 2006).

Conversely, using standard MLT, the envelope becomes dynamically unstable and our calculations encounter numerical difficulties just as the star leaves its Hayashi track, when the core has a mass of $1.32\,{\rm M}_\odot$. By extrapolating the core-growth rate, the star would likely still reach the Chandrasekhar limit (see Woosley 2019, for a similar conclusion). More realistically, binary interactions would easily remove the envelope at this stage, as its binding energy corresponds to only a minuscule fraction of the orbital energy reservoir.

Interestingly, the combination of enhanced mass loss and vigorous burning, leads to the complete depletion of helium in the envelope. Following the thermal flash, the small residual envelope contracts and the wind ceases completely for the last ∼5,000 yr (Figure 1). Our model stops when the star has a mass of $1.39\,{\rm M}_\odot$ (see Sec. 2.3).

The surface evolution of M2 is similar (Figure 1). Here, the star expands twice, first for ∼5,000 yr, and then very briefly for some ∼500 yr, reaching a maximum size of $300\,{\rm R}_\odot$. The mass-loss rate however, always remains below $10^{-6}\,{\rm M}_\odot\,{\rm yr}^{-1}$. In M2, carbon ignites near mass coordinate $1\,{\rm M}_\odot$, just as the star begins to develop an SAGB structure. The flame is quenched after only $0.1\,{\rm M}_\odot$ of material has been converted to NeO, leaving behind a hybrid CO/NeO structure. Independently of whether this composition profile survives (Brooks et al. 2017), the amount of residual carbon is substantial. This model has a final mass of $1.37\,{\rm M}_\odot$.

To summarise, during the final evolutionary stages, both models are helium depleted and nearing $M_{\rm Ch}$. The ability of the core to grow in mass depends somewhat on the uncertain mass-loss rate during the final burning phases. If the envelope is lost too early during the SAGB phase (which does not seem to be the case), then the two stars would leave be-

hind white dwarfs with masses $\leq 1.38\,M_\odot$, and ONe and CO/ONe composition respectively.

Conversely, if the envelope is retained for long enough, then the central density increases sufficiently to trigger either electron captures on ^{24}Mg or central carbon ignition. In the following section we examine the evolution of the core during this phase.

2.3. *Late evolution and thermonuclear runaway*

Figure 2 gives an overview of the central density and temperature evolution for models M1 and M2 .

Following the main carbon-burning episode, both stars continue to contract, while cooling due to neutrino emission. As shell burning intensifies, compressional heating eventually balances off neutrino losses, at $\log_{10}(\rho_c/\mathrm{gr\,cm^{-3}}) \simeq 8.3$ and 8.0 for M1 and M2 respectively. The subsequent evolution depends on the composition. For M1, the degenerate core is composed mostly of neon and oxygen. The most abundant isotopes have $X(^{16}\mathrm{O}) \simeq 0.43$; $X(^{20}\mathrm{Ne}) \simeq 0.42$; $X(^{24}\mathrm{Mg}) \simeq 0.1$; $X(^{12}\mathrm{C}) \simeq 0.011$; $X(^{23}\mathrm{Na}) \simeq 0.037$; $X(^{25}\mathrm{Mg}) \simeq 0.001$. Between $\log_{10}(\rho_c/\mathrm{gr\,cm^{-3}}) = 9.05$ and 9.25, the temperature drops to $\log_{10}(T_c/\mathrm{K}) \simeq 8.2$ due to ^{25}Mg^{25}Na and ^{23}Na^{23}Na direct Urca reactions. At higher densities, neutrino cooling ceases completely, and the temperature rises again, along the adiabatic curve shown in Figure 2.

When $\log_{10}(\rho_c/\mathrm{gr\,cm^{-3}}) = 9.65$, exothermic electron captures on ^{24}Mg and ^{24}Na start occurring at a substantial rate, raising the temperature adequately to ignite carbon. In turn, this triggers oxygen burning and a thermonuclear runaway at $\log_{10}(\rho_c/\mathrm{gr\,cm^{-3}}) = 9.77$. This ignition density is much lower than the $\log_{10}(\rho_c/\mathrm{gr\,cm^{-3}}) \geq 9.97$ typically expected for oxygen deflagrations in pure NeO cores (Jones et al. 2019). As a consequence, severe deleptonization due to ^{20}Ne electron captures are avoided.

M2 is composed mostly of carbon and oxygen, with $X(^{12}\mathrm{C}) = 0.38$ and $X(^{16}\mathrm{O}) = 0.60$ respectively. Here, ^{23}Na is not abundant enough to cause substantial cooling. Consequently, carbon, which is significantly more abundant compared to M1, ignites at $\log_{10}(\rho_c/\mathrm{gr\,cm^{-3}}) = 9.26$.

The evolution following central oxygen ignition is not adequately modeled in our 1D simulations. M2 will most likely disrupt in a SN Ia, as the composition and ignition conditions resemble closely those found in standard CO WD progenitors (Nomoto 1982). While the fate of M1 is less certain, a thermonuclear explosion is also the most likely outcome: firstly, the available nuclear energy is sufficient to unbind the star (see below). Secondly, the ignition density is not too much higher than the $\log_{10}(\rho_c/\mathrm{gr\,cm^{-3}}) \simeq 9.3 - 9.7$ expected for CO WD progenitors. Hence, the deflagration ashes will likely be buoyant, leading to expansion, which will in turn limit the deleptonization rate. This hypothesis is strongly supported by 3D hydrodynamic simulations of ECSN deflagrations by Jones et al. (2019): their least compact progenitor ingites at $\log_{10}(\rho_c/\mathrm{gr\,cm^{-3}}) = 9.90$ but still manages to eject $\sim 1\,M_\odot$ of material. Similarly, Marquardt et al. (2015) simulate ONe WD detonations at lower densities and demonstrate that the explosion is practically identical to a typical SN Ia. Interestingly in our 1D simulations, both models experience significant expansion. This is most likely the result of (over-)efficient convection, which also homogenizes the inner $\sim 1\,M_\odot$ of the core.

2.4. *Energetics and nucleosynthesis*

Figure 3 shows the density profiles of M1 and M2 at maximum compactness, and at the end of our simulations. At the onset of oxygen ignition, M1 and M2 have internal energies (gravitational+thermal) of -5.76 and -5.16 erg, and average electron fractions of $Y_e = 0.496$ and 0.499 for M1 and M2 respectively. If these progenitors were to produce an SN Ia of typical composition of $\sim 0.7\,M_\odot$ of nickel and iron and $0.6\,M_\odot$of Si-group elements, the corresponding kinetic energies would be $E_{\rm M1} \simeq 0.83$ and $E_{\rm M2} \simeq 1.17 \times 10^{51}$ erg, consistent with observations. Obviously, the nucleosynthesis yields depend on the actual Y_e and density profiles during explosive burning. If M1 achieves nuclear statistical equilibrium (NSE) without significant expansion and deleptonization, then it would produce mostly stable iron-peak elements and $\sim 0.3\,M_\odot$ of ^{56}Ni, resulting in a sub-luminous explosion. On the other hand, if NSE is achieved after an initial deflagration (Figure 3), then up to $1\,M_\odot$ of ^{56}Ni can be produced, with only moderate amounts of iron. Similarly, M2 could produce up to $1.3\,M_\odot$ of iron elements if it doesn't expand any further.

3. EXPECTED RATES AND DELAY TIMES

A useful proxy for the potential (C)NeO/SN Ia connection would be a comparison between the Hubble-integrated number of SNe Ia, $n_{\rm SN\,Ia}$, and the expected frequency of stripped near-Chandrasekhar mass (C)NeO cores, $n_\star$. Here, we provide an order-of-magnitude estimate to demonstrate that the two may indeed be similar.

To first order, $n_\star$ would be some fraction of the initial star-forming mass that will end up creating (C)NeO cores. Since the envelope needs to be removed before the onset of core helium burning, these stars would also need to be members of close binary systems, thus:

$$n_\star \simeq f_{\rm bin} \times f_{\rm int} \times n_{\rm (C)NeO}. \quad (1)$$

Here, $f_{\rm bin} \simeq 0.7$ (Sana et al. 2012) is the stellar binary fraction, $n_{\rm (C)NeO}$ is the total number of stars able to form (C)NeO cores, and $f_{\rm int} \leq 1$ is an efficiency factor to account for the impact of binary interactions (see below).

For binaries, the number of systems with ZAMS masses within a certain range (Figure 4) is:

$$n(m_1, m_2) dm_1 dm_2 = m_1^\alpha q^\kappa dm_1 dq, \quad (2)$$

where m_1 is the mass of the primary, here defined as the initially more massive star, $q \equiv m_2/m_1 \leq 1$ is the mass ratio, and a, κ depend on the initial mass function (IMF) and

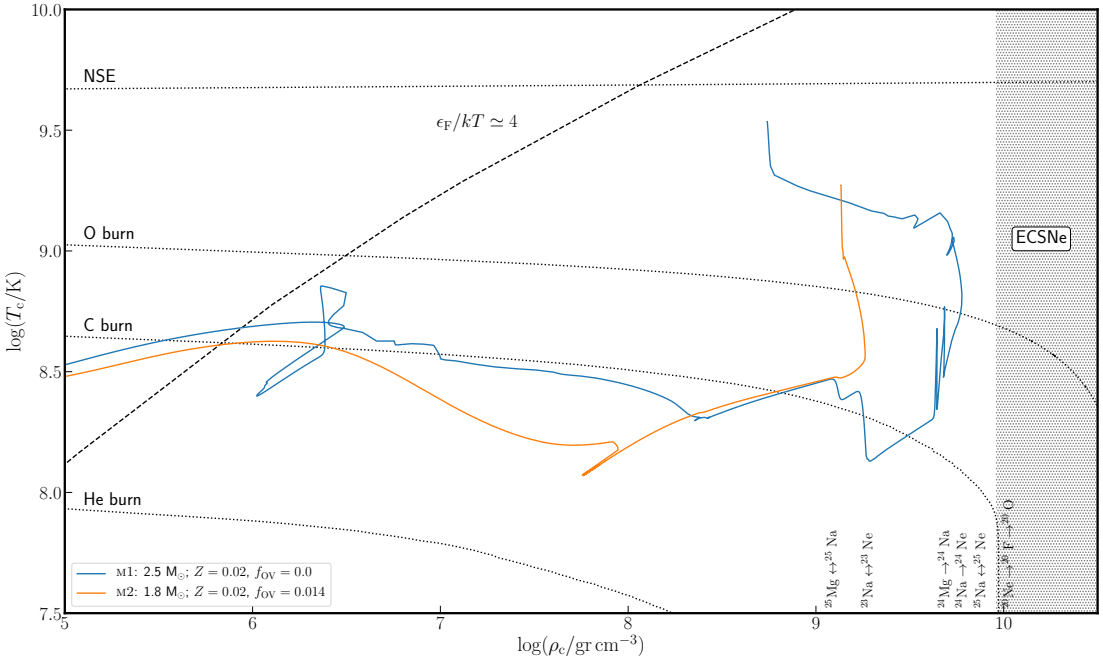

Figure 2. Evolution of the core density and temperature for M1 and M2. The dashed line shows the approximate boundary for electron degeneracy. Burning thresholds for a 100% abundace of the corresponding species are indicated with dotted lines. The NSE threshold assumes an equilibrium timescale of 1 s.

mass-ratio distribution respectively. Integrating, one finds:

$$N = \int_{m_{\rm min}}^{m_{\rm max}} \int_{q_1}^{q_2} m_1^{\alpha} q^{\kappa} dm_1 dq = f \frac{(m_{\rm min}^{\alpha+1} - m_{\rm max}^{\alpha+1})(q_1^{\kappa+1} - q_2^{\kappa+1})}{(\alpha+1)(\kappa+1)}, \quad (3)$$

where f is an appropriate normalization factor. Naively, one would expect the largest contribution from stars that, in isolation, would be able to evolve to the SAGB, viz. stars with ZAMS masses between ~ 7 and $11\,\mathrm{M}_\odot$ (Farmer et al. 2015). Since accretion is not required to trigger an explosion, *all* primaries and secondaries inside this mass range can potentially contribute to $n_\star$. Hence, $(m_{\rm min}, m_{\rm max}) = (7, 11)\,\mathrm{M}_\odot; (q_1, q_2) = (0, 1)$ for the primaries (blue region in Figure 4), and $(m_{\rm min}, m_{\rm max}) = (11, 125)\,\mathrm{M}_\odot; (q_1, q_2) = (7/11, 1)$ for the secondaries (red region). For normalization, we consider all systems within $(m_{\rm min}, m_{\rm max}) = (0.1, 125)\,\mathrm{M}_\odot$. Adopting a Chabrier (2005) IMF with $a = -2.35$ for $m_1 \geq 1$, and a $q-$distribution with $k = -0.1$ (Sana et al. 2012), Eq. 3 yields, $n_{\rm (C)NeO} \times f_{\rm bin} \simeq 5.42 \times 0.7 = 0.0039$ stars per $\mathrm{M}_\odot$ formed, with the largest contribution ($\sim 80\%$) expected from primaries. For $f_{\rm int} \simeq 1$, $n_\star$ would therefore exceed the number of SN Ia integrated over a Hubble time, $n_{\rm SN\,Ia} \simeq 0.002\,\mathrm{M}_\odot{}^{-1}$ (Maoz et al. 2014).

However, $f_{\rm int}$ is most likely smaller than unity. Firstly, only a fraction of the progenitor binary population will create naked helium stars. Most systems within the hatched regions of Figure 4 will transfer mass to their less massive companions after leaving the main sequence. For the majority of these cases, this process will be dynamically unstable, therefore leading to the removal of the envelope. If this process is indeed efficient, one would expect at least half of the stars to lose their envelopes, hence, conservatively, $f_{\rm int} \lesssim 0.5$ (Sana et al. 2012).

Following the stripping of the envelope, any subsequent interaction should be sufficiently delayed, for the core to reach $M_{\rm Ch}$. The post-CE orbital period distribution would generally favor slightly more compact configurations. Hence, only some fraction of the systems will be wide enough to allow a second CE episode after the progenitor has expanded beyond $\sim 100\,\mathrm{R}_\odot$. Nonetheless, a fraction of the closer binaries that will undergo stable case BB Roche-lobe overflow (RLO), could still leave behind stripped (C)NeO cores of sufficiently high mass. For instance, the simulations of Tauris et al. (2015) suggest that a considerable number of helium-free (C)NeO proto-WDs with $m \simeq M_{\rm Ch}$ can be produced via this channel.

Considering some of the major uncertainties, conservatively, we expect: $0.1 \lesssim f_{\rm int} \lesssim 0.5$. Taking into account

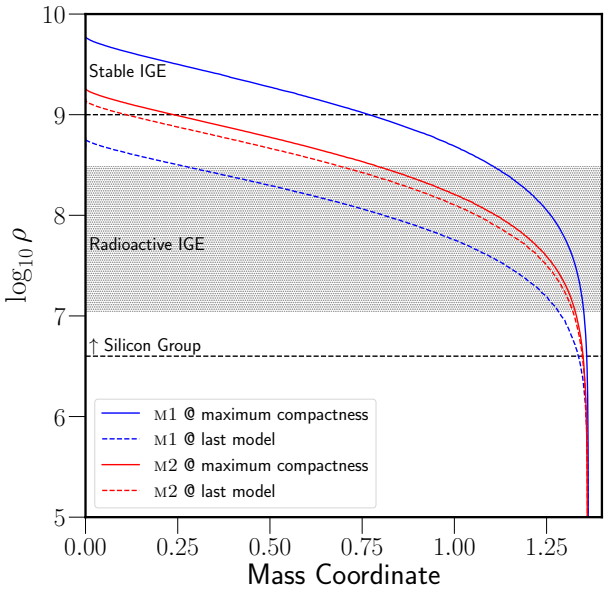

Figure 3. Density profiles at maximum compactness (solid lines) and at the end of our MESA calculations (dashed lines). Regions indicating approximate burning regimes as in Seitenzahl & Townsley (2017).

further ambiguities in the IMF and initial configurations, we conclude that $0.05 \lesssim n_\star/n_{\rm SN\,Ia} \lesssim 1$.

Obviously, the above estimate omits most interactions that could move systems in and out of the hatched regions in Figure 4. Of particular importance may be interactions occurring before the helium-burning phase, as there are roughly three times as many systems with a total mass larger than $7\,{\rm M}_\odot$ than there are stars within the hatched regions of Figure 4. A fraction of this population can contribute significantly to the observed rate, after interacting via Case A/B RLO. Additional contributions may come from higher-order multiple systems and/or dynamical interactions in dense environments.

Besides the integrated number of SNe Ia, a property that is more challenging to match is the evolution of the SN Ia rate with cosmic time. SNe Ia from this channel would have delay times dominated by the main sequence lifetime of the progenitors, i.e. of order 25 to 78 Myr, for stars with ZAMS masses between 7 and 11 $\rm M_\odot$. Binaries interacting via early Case A RLO prior to the removal of the envelope, could contribute events up to ~ 350 Myr following star formation.

These delay times could help account for the high SN Ia rates in star-forming galaxies (Maoz & Badenes 2010; Claeys et al. 2014b). However, some variant of the DD channel would still be required to explain events with much longer delay times.

4. SUMMARY

We have shown that stars able to form degenerate (C)NeO cores after losing their hydrogen envelopes, are likely to explode as SNe Ia instead of undergoing a core-collapse ECSN. For NeO compositions, the runaway seems to be triggered by the ignition of residual carbon following electron captures on ^{24}Mg, which in turn leads to explosive oxygen burning at densities below $10^{9.77}\,{\rm gr\,cm^{-3}}$ (Sections 2). For hybrid CO/NeO cores, ignition is triggered by core compression, at a density of $10^{9.26}\,{\rm gr\,cm^{-3}}$, similar to what is expected for CO WD deflagrations. For either case, the conditions at the onset of oxygen burning are such that the energetics could resemble closely a typical SNe Ia (Section 2.4). It would be worth considering whether the differences in density and composition could lead to distinct nucleosynthetic signatures that would help distinguish these progenitors and/or contribute uniquely to the chemical evolution of the Galaxy (in analogy to Jones et al. 2019, for ECSNe).

The frequency of the corresponding progenitor systems is sufficient to account for a considerable fraction of the observed SN Ia rate (Section 3). Since, the bulk of events would occur only $\sim$ 50 Myr after star formation, this channel is mostly relevant to active late-type galaxies. The shorter delay times compared to traditional SN Ia scenarios, opens further interesting avenues for constraining this model, e.g. with low-metallicity stars.

A similar SN Ia channel has been proposed by Waldman & Barkat (2006) and Waldman et al. (2008), who have also demonstrated that some helium stars with (C)NeO cores can explode before any significant deleptonization occurs. However, these authors do not follow the final evolution stages, and their progenitors still retain a small He-rich envelope at the end. While here we demonstrate that the helium envelope is likely lost only after the core has grown to $M_{\rm Ch}$, its evolution remains a major uncertainty for this progenitor channel. If helium is removed sufficiently early, e.g. due to binary interactions or dynamical instabilities, then this channel would instead create sub-$M_{\rm Ch}$ (C)NeO WDs. In spite of the mass-loss uncertainties, if viable, this channel would help explain some of the observed SN Ia diversity. Since either star in binary system may potentially explode as a SN Ia without accreting from its companion, the resulting events can resemble setups expected in both SD and DD scenarios. Explosions resulting from the explosion of the secondary, would follow a first core-collapse SN. This could lead to SN Ia remnants with no luminous surviving stars, high proper motions due to a kick from the first SN (like the Kepler remnant, Chiotellis et al. 2012), and possibly associated with a neutron star. Since the envelope can be removed either due to winds, case-BB mass transfer, or a common envelope event, some diversity is also expected in the SN environment. In turn this would influence bot the appearance of the explosion and the evolution of the SN remnant.

Finally this channel seems relevant to other emerging correlations, e.g. the one found between SN locations and the velocity of Si features, or the apparent correlation between SN Ia rate and IMF variations at low masses (Maoz et al. 2014).

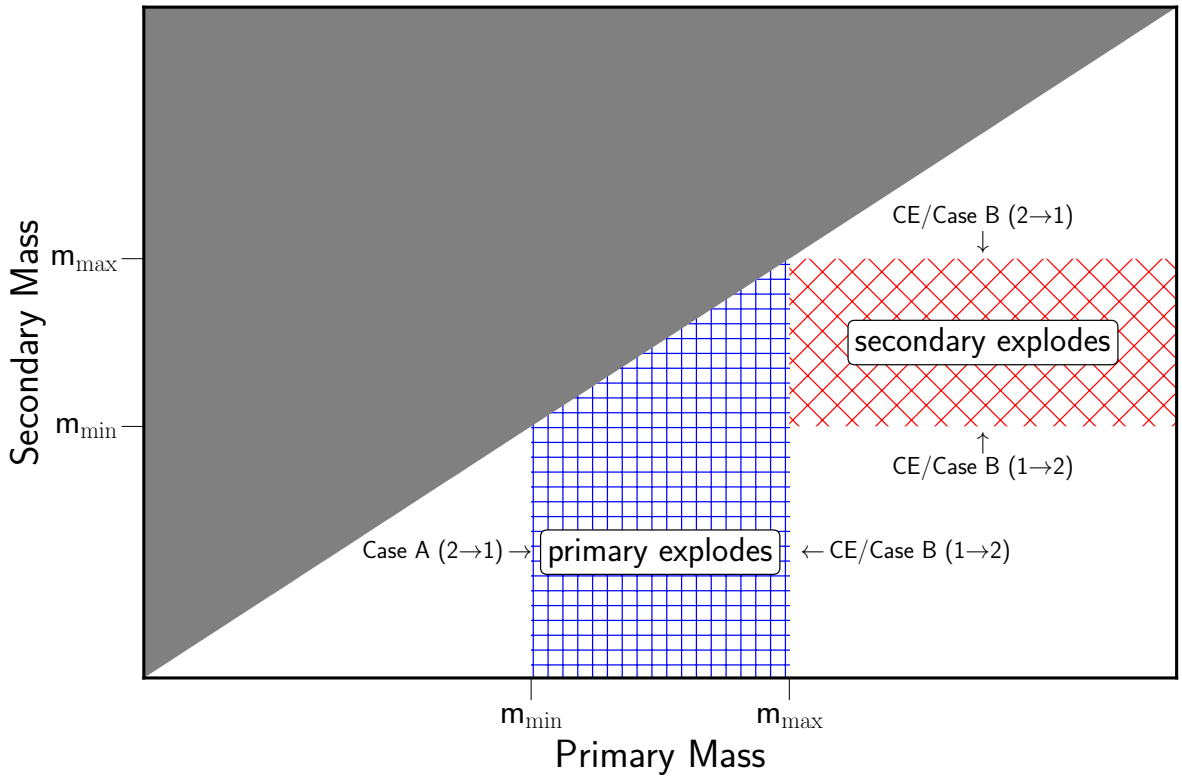

Figure 4. Overview of the different systems contributing to the SN Ia channel discussed here, on the mass-mass plane (see text).

We thank Philipp Podsiadlowski, Friedrich Röpke, Samuel Jones and Josiah Schwab for useful discussions. This research made extensive use of NASA's ADS.

Software: MESA[2] (Paxton et al. 2011, 2013, 2015, 2018), Astropy[3] (Astropy Collaboration & Astropy Contributors 2018) , MESAplot (Farmer 2018)

REFERENCES

Astropy Collaboration, & Astropy Contributors. 2018, The Astronomical Journal, 156, 123

Bochenek, C. D., Dwarkadas, V. V., Silverman, J. M., et al. 2018, Monthly Notices of the Royal Astronomical Society, 473, 336

Brooks, J., Schwab, J., Bildsten, L., Quataert, E., & Paxton, B. 2017, The Astrophysical Journal, 834, L9

Chabrier, G. 2005, The Initial Mass Function 50 Years Later, 327, 41

Chanlaridis, S., Antoniadis, J., Gräfener, G., & Langer, N. 2019, in prep.

Chiotellis, A., Schure, K. M., & Vink, J. 2012, Astronomy & Astrophysics, 537, A139

Churazov, E., Sunyaev, R., Isern, J., et al. 2014, Nature, 512, 406

Claeys, J. S. W., Pols, O. R., Izzard, R. G., Vink, J., & Verbunt, F. W. M. 2014a, Astronomy & Astrophysics, 563, A83

—. 2014b, Astronomy and Astrophysics, 563, A83

Cox, J. P., & Giuli, R. T. 1968, Principles of stellar structure

Cyburt, R. H., Amthor, A. M., Ferguson, R., et al. 2010, The Astrophysical Journal Supplement Series, 189, 240

Denissenkov, P. A., Herwig, F., Truran, J. W., & Paxton, B. 2013, The Astrophysical Journal, 772, 37

Farmer, R. 2018, rjfarmer/mesaplot

Farmer, R., Fields, C. E., & Timmes, F. X. 2015, The Astrophysical Journal, 807, 184

Filippenko, A. V., Richmond, M. W., Matheson, T., et al. 1992, The Astrophysical Journal, L5

Grevesse, N., & Sauval, A. J. 1998, Space Science Reviews, 85, 161

[2] http://mesastar.org
[3] http://www.astropy.org

Gutierrez, J., Garcia-Berro, E., Iben, I., et al. 1996, The Astrophysical Journal, 459, 701

Harris, C. E., Nugent, P. E., & Kasen, D. N. 2016, The Astrophysical Journal, 823, 100

Howell, D. A., Sullivan, M., Nugent, P. E., et al. 2006, Nature, 443, 308

Jones, S., Röpke, F. K., Fryer, C., et al. 2019, Astronomy and Astrophysics, 622, A74

Kasen, D. 2010, The Astrophysical Journal, 708, 1025

Kippenhahn, R., Ruschenplatt, G., & Thomas, H.-C. 1980, Astronomy and Astrophysics, 91, 175

Langer, N., Fricke, K. J., & Sugimoto, D. 1983, Astronomy and Astrophysics, 126, 207

Livio, M., & Mazzali, P. 2018, Physics Reports, 736, 1

Maoz, D., & Badenes, C. 2010, Monthly Notices of the Royal Astronomical Society, 407, 1314

Maoz, D., Mannucci, F., & Nelemans, G. 2014, Annual Review of Astronomy and Astrophysics, 52, 107

Marquardt, K. S., Sim, S. A., Ruiter, A. J., et al. 2015, Astronomy and Astrophysics, 580, A118

Nomoto, K. 1982, The Astrophysical Journal, 253, 798

Nomoto, K., & Kondo, Y. 1991, The Astrophysical Journal, 367, L19

Owocki, S. P., Gayley, K. G., & Shaviv, N. J. 2004, The Astrophysical Journal, 616, 525

Paxton, B., Bildsten, L., Dotter, A., et al. 2011, The Astrophysical Journal Supplement Series, 192, 3

Paxton, B., Cantiello, M., Arras, P., et al. 2013, The Astrophysical Journal Supplement Series, 208, 4

Paxton, B., Marchant, P., Schwab, J., et al. 2015, The Astrophysical Journal Supplement Series, 220, 15

Paxton, B., Schwab, J., Bauer, E. B., et al. 2018, The Astrophysical Journal Supplement Series, 234, 34

Ruiz-Lapuente, P., Jeffery, D. J., Challis, P. M., et al. 1993, Nature, 365, 728

Sana, H., de Mink, S. E., de Koter, A., et al. 2012, Science, 337, 444

Sato, Y., Nakasato, N., Tanikawa, A., et al. 2015, The Astrophysical Journal, 807, 105

Schwab, J., Bildsten, L., & Quataert, E. 2017, Monthly Notices of the Royal Astronomical Society, 472, 3390

Seitenzahl, I. R., & Townsley, D. M. 2017, Nucleosynthesis in Thermonuclear Supernovae, 1955

Siess, L. 2006, Astronomy and Astrophysics, 448, 717

Smith, N., & Owocki, S. P. 2006, ApJL, 645, L45

Suzuki, T., Toki, H., & Nomoto, K. 2016, \apj, 817, 163

Takahashi, K., Yoshida, T., & Umeda, H. 2013, The Astrophysical Journal, 771, 28

Taubenberger, S. 2017, Handbook of Supernovae, 317

Tauris, T. M., Langer, N., & Podsiadlowski, P. 2015, Monthly Notices of the Royal Astronomical Society, 451, 2123

van Kerkwijk, M. H., Chang, P., & Justham, S. 2010, The Astrophysical Journal, 722, L157

Waldman, R., & Barkat, Z. 2006, Ph.D. Thesis

Waldman, R., Yungelson, L. R., & Barkat, Z. 2008, in Astronomical Society of the Pacific Conference Series, Vol. 391, Hydrogen-Deficient Stars, ed. A. Werner & T. Rauch, 359

Woosley, S. E. 2019, The Astrophysical Journal, 878, 49

3.2 Helium Stars as Progenitors of Thermonuclear Supernovae

In this section, we further explore the progenitor channel of SNe-Ia we described in section 3.1, by creating series of stellar models with various values of metallicity and overshoot mixing. We elaborate on the importance of residual carbon found in ONe cores, in initiating a thermal runaway leading to the disruption of the star.

DRAFT VERSION AUGUST 11, 2019
Typeset using LaTeX **twocolumn** style in AASTeX62

Helium Stars as Progenitors of Thermonuclear Supernovae: Dependence on Metallicity and Overshooting

S. CHANLARIDIS,[1] J. ANTONIADIS,[1,2] G. GRÄFENER,[1] AND N. LANGER[1,2]

[1]*Argelander-Institut für Astronomie, University of Bonn, Auf dem Hügel 71, D-53121 Bonn, Germany*
[2]*Max-Planck-Institut für Radioastronomie, Auf dem Hügel 69, D-53121 Bonn, Germany*

(Received XXX; Revised YYY; Accepted ZZZ)

Submitted to AAS

ABSTRACT

Type Ia supernovae (SNe Ia) are luminous optical transients characterized by the absence of hydrogen and helium in their spectra. The majority of SNe Ia are thought to result from the thermonuclear disruption of white dwarfs, which is triggered by mass accretion in a binary system. However, both the details of the explosion mechanism and the exact nature of the progenitor systems remain a topic of debate. Recent results from wide-field transient surveys, suggest that SNe Ia are far more diverse than previously thought. This diversity could be the result of varied progenitor systems. We have discovered a novel SN Ia progenitor channel, in which a thermonuclear explosion is initiated during the late evolution of stripped helium stars with masses between $\sim 1.8-2.7\,M_\odot$ which are frequently produced from the mass donors in interacting massive, close binaries. This mechanism does not require accretion from the binary companion and therefore may contribute significantly to the SN Ia rate in star-forming galaxies (i.e. at early delay times).

Keywords: stars: evolution — white dwarfs — supernova: general — nuclear reactions, nucleosynthesis

1. INTRODUCTION

Helium stars (He stars) are the exposed, naked cores of hydrogen deficient stars that have lost their hydrogen-rich mantle either via stellar winds or mass transfer episodes, if it happens to be part of a binary system. For progenitor stars in the initial mass range $M_i \approx 8 - 10\ M_\odot$, carbon will be ignited in a shell, following the depletion of helium supply in their cores. Responsible for this off-centre ignition is significant neutrino cooling that occurs deep in the stellar core, and shifts the location of maximum temperature (temperature inversion) to the aforementioned shell. This marks the transition of the star toward the super-asymptotic giant branch (SAGB). The heat generated from the burning shell creates a subsonic carbon-burning front ("C-flame") that propagates inward. The physical properties of such a deflagration have been the subject of various studies (e.g. Timmes et al. 1994; Siess 2006, 2009; Denissenkov et al. 2013; Farmer et al. 2015) and show a strong dependency on the adopted initial parameters.

As this C-flame moves toward the centre, it will process the material of the partially degenerate carbon-oxygen (CO) core converting it into an oxygen-neon (ONe) core. The subsequent evolution that will determine the final fate of the star, depends on the interplay between the core mass growth rate and the mass loss rate. If shell burning allows the core to reach the critical mass value of $\sim 1.37\ M_\odot$ (Nomoto 1984), the central density becomes sufficiently high ($\rho_c \sim 10^{9.95}$ gr cm^{-3}) for electron captures on ^{24}Mg and ^{20}Ne nuclei to ensue, essentially reducing the pressure in the interior, and ultimately leading to the collapse of the core; this is referred to as *electron capture supernova* (ECSN). The end product of an electron capture induced collapse would be a low-mass neutron star formed from a dim supernova (e.g. Fischer et al. 2010, and references therein) with relatively low explosion energy, which imparts only a small natal kick to the remnant (Knigge et al. 2011; Jones et al. 2013; Jones et al. 2016) compared to the iron core collapse (Fe-CCSN) channel.

On the other hand, if the central density does not reach the threshold for electron captures on the most abundant species, the star will shed its envelope before the core reaches the Chandrasekhar mass limit (M_{ch}), and end up as an ONe white dwarf (ONe WD). However, if the ONe WD is in a close binary system, it can evolve to a supernova following a similar path as the one described above. This can be realized with the transfer of mass from the companion star onto the surface of the WD, allowing it to grow near the Chandrasekhar mass and leave behind a neutron star, a scenario that is known as *accretion-induced collapse* (AIC) (e.g. Nomoto & Kondo 1991; Schwab et al. 2015; Brooks et al. 2017; Schwab & Rocha 2019).

Corresponding author: Savvas Chanlaridis
schanlar@astro.uni-bonn.de

1.1. *Thermonuclear Supernovae*

Due to lack of a hydrogen envelope, the collapsing core of a He star would be observed as a type Ib/c supernova, depending on the degree of stripping as has been shown by Tauris et al. (2013, 2015). In the case of normal SAGB stars that retain a hydrogen-rich mantle, the spectral lines could resemble the ones found in types IIn-P supernovae (see Moriya et al. 2014, for details).

Nonetheless, one should keep in mind that by the time the effects of electron captures on nuclei cannot be neglected, the necessary pressure gradient against gravity is provided by a strongly degenerate electron gas. For degenerate matter, pressure does not depend on the temperature thus the star can no longer respond to a temperature increase by expanding its outer layers. Since thermonuclear reaction rates are extremely sensitive to temperature variations, under such degenerate conditions, even a small increase of temperature caused by ignition of the existing nuclear fuel, could alter the nuclear burning rate dramatically resulting in a thermal runaway.

Whether the ONe WD undergoes core collapse or experiences a thermonuclear explosion depends on the timescale of electron captures versus the timescale of nuclear energy release. Since electron captures become energetically favorable only above specific values of central density, the ignition location of explosive nuclear burning plays a major role to the final result. Indeed, Jones et al. (2016) have demonstrated that for low ignition density, the core does not collapse into a neutron star but rather explodes leaving behind bound remnants.

The consideration above is consistent with the explosion mechanisms (e.g. single degenerate model) related to type Ia supernovae (for recent reviews see Hillebrandt & Niemeyer 2000; Wang & Han 2012; Wang 2018; Livio & Mazzali 2018). It becomes apparent that ECSNe could originate from a variety of progenitor systems either in single or binary configuration, and the connection between the progenitor and the final outcome is far from trivial.

1.2. *The Urca process*

The term "Urca-processes" was introduced by Gamow & Schoenberg (1941) in order to describe energy losses from neutrino emission. It consists of two weak nuclear reactions: an electron capture that operates on a mother nucleus $M \equiv (A, Z)$ forming a more neutron-rich, daughter isobar $D \equiv (A, Z-1)$

$$(A, Z) + e^- \longrightarrow (A, Z-1) + \nu_e \tag{1}$$

and a beta-decay transition of D back to M

$$(A, Z-1) \longrightarrow (A, Z) + e^- + \bar{\nu}_e \tag{2}$$

where A and Z denote respectively the mass number and the atomic number of the nucleus. The mother-daughter pair $({}^{A}_{Z}M, {}^{A}_{Z-1}D)$ can be referred to as "Urca nuclei".

As central density increases, the Fermi energy ϵ_F (or equivalently the electron chemical potential, μ_e) of the relativistic, degenerate Fermi gas prevails over the threshold energy E_t of a given Urca nuclei pair (i.e. the difference between the rest masses of M and D, given by the Q value for a ground state to ground state transition), and electron captures will commence promptly. The associated reaction rates (λ^+, λ^-), and neutrino energy losses (L^+, L^-) per nucleon for equations 1, 2 respectively, have been calculated by Tsuruta & Cameron (1970) and exhibit a strong sensitivity on temperature and density. Therefore, Urca processes become important only for a narrow range of stellar plasma properties, defining a thin Urca shell in which they operate (where $\epsilon_F = E_t$).

Paczyński (1972) argued that during the simmering phase of a CO WD, the energy released from carbon burning would not be able to be transferred efficiently via radiative means leading to a convective core that could engulf the Urca shell (convective Urca). Ultimately, the Urca neutrinos[1] would carry away enough energy to delay the dynamical runaway and forcing the core to move to higher densities thus, collapsing into a neutron star. However, Bruenn (1973) challenged this notion by showing that Urca processes can also have destabilizing effects by generating heat, if convective motions re-position the relevant nuclei at some distance from the Urca shell. In these non-equilibrative states, if e-capture dominates over the β-decay (i.e. if $\rho > \rho_{\rm th}$), the captured electron creates a "hole" in the Fermi sea and forces another electron to drop from the Fermi surface in order to fill the gap, resulting in heating. On the other hand, if $\rho < \rho_{\rm th}$, β-decay liberates electrons with excess thermal energy that also results in heating. Therefore, convective Urca processes can either play a major role as local cooling mechanisms (at mass coordinate in the vicinity of the Urca shell where both reactions are in equilibrium) or contribute to heating outside the Urca shell.

The effect of convective Urca processes on stellar interiors remain still an open question and provides up to this day fertile ground for debate. For a more detailed analysis, and fruitful discussion on the physics and importance of Urca process we refer to the work of Paczyński (1973); Barkat & Wheeler (1990); Stein et al. (1999); Lesaffre et al. (2005); Waldman & Barkat (2007); Denissenkov et al. (2015); Schwab et al. (2017).

The structure of this paper is organized as follows. In Section 2, we present the input physics we used to model the evolution of our He-stars. In Section 3, we discuss our results and their implications to our current state of knowledge. Section 4 provides a summary of our results and necessary future work.

[1] Here we use the term "neutrinos" to refer both to neutrinos and antineutrinos interchangeably.

2. STELLAR EVOLUTION CODE AND INITIAL PARAMETER SPACE

We performed numerical calculations using the one dimensional, stellar evolution code **M**odules for **E**xperiments in **S**tellar **A**strophysics (MESA), version - r10398 (Paxton et al. 2011, 2013, 2015, 2018, 2019).

2.1. *Physical assumptions*

Our grid consists of 252 single He stars in the mass range $0.8 \leq M/M_{\odot} \leq 3.5$ with a step of 0.1. Evolutionary calculations begin from the pre-main sequence phase with a uniform initial composition. In order to study the effects of metallicity, we create a series of models with low ($Z = 0.0001$), intermediate ($Z = 0.001$), and solar metallicity ($Z \equiv Z_{\odot} = 0.02$). Similarly, for varying the efficiency of overshooting we create series with no overshooting ($f_{\rm ov} = 0.0$), and overshoot mixing ($f_{\rm ov} = 0.014$, $f_{\rm ov} = 0.016$) across all convective boundaries. The free parameter $f_{\rm ov}$ is defined in Herwig (2000) as a fraction of the local pressure scale height, H_p, and is connected to the diffusion coefficient, $D_{\rm OV}$, via the relation given by equation 3, where z is the geometric distance from the edge of the convective zone.

$$D_{\rm OV} = D_0 \exp\left(-\frac{2z}{H_v}\right), \qquad H_v = f_{\rm ov} \cdot H_p \tag{3}$$

The choice of an adequate nuclear network and accurate weak rates are aspects of paramount importance in our considered mass-range, since we expect substantial amounts of ^{23}Na, ^{25}Mg, and ^{27}Al to be produced after the carbon burning phase. Urca process operating on those odd-mass-number nuclei can alter the energy balance with a significant impact upon the thermal structure of the core. For this reason, we construct a nuclear reactions network that consists of forty-three nuclear species, including important NeNa and MgAl cycles, and relevant weak reactions for several Urca pair isotopes. Finally, we incorporate the special weak rates from Suzuki et al. (2016).

We considered ion and electron screening corrections as described in Potekhin et al. (2009) and Itoh et al. (2002) respectively. To account for an enhanced carbon-oxygen mixture as a result of helium burning, we used the Type-2 OPAL Rosseland mean opacity tables (Iglesias & Rogers 1996). For the equation of state blending we followed the options suggested by Schwab et al. (2017).

Convection was treated according to the standard mixing-length theory prescription of Henyey et al. (1965) with a mixing-length parameter of $\alpha_{\rm ML} = 2.0$. Furthermore, we used the Ledoux criterion for convective instability adopting an efficiency parameter of $\alpha_{\rm SEM} = 1.0$ for semi-convection (Langer 1991), and a diffusion coefficient $D_{\rm TH} = 1.0$ for thermohaline mixing (Brown et al. 2013). Both semi-convection and thermohaline mixing are treated by MESA as diffusive processes (Langer et al. 1983; Kippenhahn et al. 1980).

Table 1. Baseline parameters for single helium stars

Parameter	Value(s)
Convection ($\alpha_{\rm ML}$)	2.0
Semiconvection ($\alpha_{\rm SC}$)	1.0
Thermohaline ($D_{\rm TH}$)	1.0
Wind scaling factor (η)	1.0
Overshooting ($f_{\rm ov}$)	0.0, 0.014, 0.016
Metallicity (Z)	10^{-4}, 10^{-3}, 0.02

Mass loss rates due to stellar winds were implemented using the "`Dutch`" wind scheme (Glebbeek et al. 2009). In our case, this implies two different rates depending on the effective temperature of the star; for $T_{\rm eff} > 10^4$ K and a surface abundance of hydrogen $X < 0.4$ by mass fraction (which is always satisfied for the models we developed), we apply the prescription of Nugis & Lamers (2000) with a scaling factor of $\eta = 1$ (canonical value). For $T_{\rm eff} < 10^4$ K the mass loss rate follows the prescription of de Jager et al. (1988).

All the baseline parameters we adopted above are summarized in Table 1, and the MESA inlists will become publicly available[2].

3. RESULTS

3.1. *Overview of the Evolution*

As it was mentioned in section 2.1, we followed the evolution of He-stars in the mass range $0.8 - 3.5$ M$_{\odot}$ starting from the pre-main sequence phase with a uniform initial composition. After the end of core helium burning, the mass fraction of carbon in the newly formed metal core is within the range $0.31 \lesssim X_C \lesssim 0.48$. Since the abundances of other species can be neglected in this stage, the mass fraction of oxygen can be taken as the complement to unity with respect the aforementioned carbon mass fraction range.

Following the depletion of helium in the core, a radiative helium-burning shell is being formed that forces the core to grow in mass. From this point, we can distinguish four different evolutionary paths; if the core mass (M$_c$) is below a lower limit M$_{\rm low}$ that depends on the adopted values for metallicity and overshooting, then carbon is never ignited and the star will end up as a carbon-oxygen white dwarf.

In the case of $\mathrm{M_{low}} \leq \mathrm{M_c} < \mathrm{M_{up}^{hyb}}$, where $\mathrm{M_{up}^{hyb}}$ is an arbitrary upper limit, carbon is ignited off-centre while the core expands and cools as a result of shell-burning. The C-flame advances inward in a series of flashes, but fails to reach the centre. The ignition location depends on both the initial mass of the star, and the carbon mass fraction. The flame quenching can be attributed to several physical mechanisms, e.g. overshoot mixing (Denissenkov et al. 2013; Chen et al. 2014;

[2] http://cococubed.asu.edu/mesa_market/inlists.html

Farmer et al. 2015), and thermohaline mixing (Siess 2009). The star in this case, will end up as a hybrid CONe white dwarf. Nevertheless, Lecoanet et al. (2016) have shown that buoyancy prevents convective plumes to penetrate into the flame since they are not dense enough, hence convective mixing is insufficient to stall a carbon flame making such hybrid WDs a non-typical product of stellar evolution.

If $M_{up}^{hyb} \leq M_c < M_{up}$, where M_{up} is once again an arbitrary upper limit, the C-flame is able to propagate all the way toward the center, forming an ONe core. However, our simulations show that in all cases, carbon is not being burned up completely, and an amount of $0.003 \lesssim X_C \lesssim 0.23$ by mass fraction is still present and distributed throughout the core. The presence of carbon may lead to explosive burning as has been suggested by (Schwab & Rocha 2019; Waldman & Barkat 2007, hereafter SR19, and WB07 respectively) and Gutiérrez, J. et al. (2005). However, both of these works investigate the effect of residual carbon in a binary system, where carbon is ignited only after a cooled-down WD, with a "frozen" carbon profile has reached the Chandrasekhar limit via accretion (AIC). The ignition density of the runaway may vary with the amount of left-over carbon, resulting in a fairly wide range of ejecta velocities and compositons. In this work, we demonstrate that the Chandrasekhar limit may be achieved via shell burning, without the need of an extended accretion phase. The runaway ignition location does not show any significant variability among our models. This is perhaps due to the nature of the degenerate cores, which are still very hot in contrast to the ONe WDs of SR19 and WB07 that have achieved homogenization via thermocompositional mixing. Additionally, the stabilizing temperature gradient in our models prohibits thermohaline mixing to re-distribute and destroy the gradient of the residual carbon profile in the core. More importantly, it prevents the destruction of the stratified core-mantle structure in hybrid CONeMg cores that would occur as the WD cools down, allowing them to grow to near Chandrasekhar masses (see also Brooks et al. 2017; Schwab & Garaud 2019).

Finally, if $M_c \geqslant M_{up}$ then carbon is ignited on-centre leading to more advanced burning stages, and ultimately the star undergoes core collapse whilst a neutron star is formed.

3.2. *Core Growth and Structure*

In the next sections, we are going to discuss the growth of hybrid and oxygen-neon cores and how their structure is affected by the metallicity environment and overshoot mixing, without concerning ourselves with the extreme cases of white dwarfs, or core collapsing stellar models.

Following the off-centre carbon burning phase, the core of the star is either dominated by carbon and oxygen which is engulfed in an ONeMg shell, or -if the C-flame reaches the centre- the degenerate core is composed primarily of oxygen and neon, with a small amount of carbon that remains unburned. In the latter case, we choose a fiducial model of 2.5 $M_\odot$, with solar metallicity and no overshooting, as representative of similar structured models, in order to demonstrate their evolution. The centre contracts and heats up whilst the

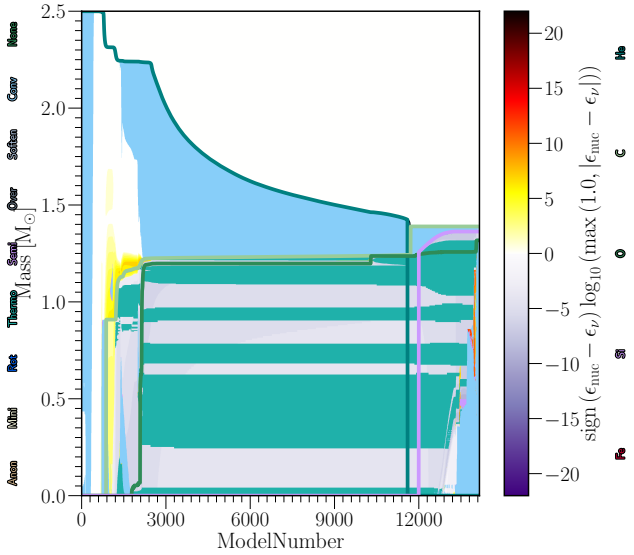

Figure 1. Kippenhahn diagram of the $2.5M_\odot$ helium star with $Z = 0.02$ and no overshooting that leads to the final structure shown in Figure 5(c). Blue areas denote regions with convection; green-coloured areas indicate thermohaline mixing. The intensity shown in the colour-bar, indicates the net energy-production rate. During the carbon simmering phase the core becomes convective.

envelope expands and develops a deep convective region that penetrates into the helium-burning shell as can be seen in Figure 1. The plot shows a cross-section of the helium star in mass coordinates along the y-axis, starting from the center and moving towards the surface of the star, as a function of stellar model number.

The core of our stellar models in the mass range $M_i = 1.8 - 2.7$ $M_\odot$ grow to near Chandrasekhar masses due to helium shell-burning, and reach a plateau of $M_c \sim 1.36 \pm 0.01$ $M_\odot$ whilst the extended He-rich envelope is easily ejected via a strong wind (see section 3.3 for discussion). Subsequently, the existing carbon in the core ignites initiating convective motions that feed the core with more carbon, and the star enters a carbon simmering phase. The energy yield from carbon burning is sufficient to raise the temperature for explosive oxygen burning under extreme degenerate conditions to occur. As a result, a thermal runaway ensues and the star which contains no helium at the time of the explosion, it would be observable as a SN Ia.

Convective overshooting leads to larger convective cores which, naturally, prolongs the time the star spends in the helium main-sequence phase and thus, lengthens its total lifetime. The reason is that an enlarged convective zone will supply the helium burning core with more fuel. The additional fuel will affect the rate at which nuclear energy is released, thus we expect higher luminosity in the cases where convective overshoot mixing is included. Moreover, the increased size of the metal core will shift the mass range for which we observe the behaviour described above, to lower initial masses. This shifting in the initial mass range caused

by the overshoot mixing and the metallicity is more evident and easily understood in Figure 3 where we display the full parameter space.

On the other hand, metallicity seems to adversely affect core growth. The effects of overshooting and metallicity on core growth can be seen in Figure 2 which shows the final core mass of our stellar models as a function of the initial mass. Missing data points correspond to models for which the code crashed before they were able to get rid of their helium envelope, thus we couldn't follow the evolution past the hot bottom burning phase and obtain a reliable estimate for the final core mass. The scattering that appears at the high-end of our grid is most likely due to the fact that these models stopped at different evolutionary stages; nonetheless, in all of those cases, the core mass has either exceeded the Chandrasekhar mass limit, or the star has developed an ONeSi structure that will eventually lead to a core-collapse, rendering these models irrelevant to our work.

Figure 3 illustrates our parameter space in a raster format. The color of each pixel indicates the composition of the star at the time the evolution was terminated. Since all models with an ONe structure (green pixels) grow to near Chandrasekhar masses, they will undergo thermal runaway as a result of the remaining carbon in their cores, avoiding this way to end up as oxygen-neon white dwarfs.

3.3. *Wind and Ejection of Inflated Envelopes*

[Gräfener]

3.4. *The Role of Residual Carbon*

3.4.1. *Oxygen-Neon Cores*

As the core is compressed, its density keeps on rising until it reaches the threshold of various Urca pairs. The ^{25}Mg - ^{25}Na, and ^{23}Na - ^{23}Ne pairs are of utmost importance in our case, and occur at densities $\log(\rho_c) \approx 9.1$, and $\log(\rho_c) \approx 9.2$ respectively. Tsuruta & Cameron (1970) have shown that the energy loss rate via Urca-cooling depends on the fourth power of temperature ($\propto T^4$), hence this effect is more prominent in our hot, young ONe cores rather than in cooled WDs.

The effect of Urca-cooling can be seen in Figure 4 where the evolution of our fiducial stellar model with initial mass of $2.5\mathrm{M}_\odot$, and solar metallicity is being displayed (blue line). The density at which carbon is ignited is illustrated with a dotted black line, taken from MESA; however, MESA assumes a 100% composition of carbon and thus, the limits shown in Figure 4 are only approximated. In our models, Urca-cooling occurs before central density reaches the threshold for carbon ignition, effectively shifting the simmering phase to higher densities, delaying the ignition of carbon, and altering the nucleosynthetic signature of the explosion.

Further compression leads to exothermic e-captures on ^{24}Mg nuclei. The generated heat ignites the residual carbon in a very localized manner due to the sensitivity of carbon reaction rates to temperature. This can be seen as a saw-tooth feature in Figure 4, where heating from carbon simmering antagonizes neutrino cooling. We did not investigate the effect of ^{24}Mg mass fraction, however Gutiérrez, J. et al. (2005) have shown that it could play a major role on the subsequent evolution.

The energy yield from carbon burning will eventually lead to dynamical burning of oxygen. Woosley et al. (2004) estimates that the end of the carbon simmering phase occurs roughly at $\log(T_c/\mathrm{K}) \approx 8.9$.

In order to mimic a carbon-free core and demonstrate the effects of residual carbon, we evolve a series of models for which we have set the rate of all carbon-consuming nuclear reactions to zero, once they reached a central density of $\log(\rho_c) = 9.0$ for the first time (grey circle in Figure 4). In this case, the compression continues achieving a balance between neutrino cooling and compressional heating. The core density continues to grow until it surpasses the threshold for e-captures on ^{20}Ne nuclei which leads to the ignition of oxygen burning. The competition between the propagating oxygen deflagration and e-captures on the post-deflagration NSE material will determine the final fate of the star. Recently, Zha et al. (2019) found that the deflagration starting from $\log(\rho_c/\mathrm{g\ cm^{-3}}) > 10.01$ leads to a collapse, reinforcing our notion that a carbon-free ONe core will, most likely, evolve towards an ECSN and ultimately in the formation of a low-mass neutron star.

3.4.2. *Hybrid CONeMg Cores*

A small number of models develop a hybrid CO/ONe structure in their core, but still reach the Chandrasekhar limit. We choose a fiducial model of $1.8\mathrm{M}_\odot$, with solar metallicity and overshooting ($f_{\mathrm{OV}} = 0.014$), in order to demonstrate the evolution of similar structured models.

Since the C-flame does not reach the centre, the Urca pairs ^{25}Mg - ^{25}Na, and ^{23}Na - ^{23}Ne, which are byproducts of carbon burning, are not in abundance. Thus, Urca cooling does not play any major role in the evolution of hybrid cores. In the absence of the aforementioned Urca pairs, the compression of the core will continue until the ignition of carbon, and explosive oxygen burning at lower densities compared to the case of of non-hybrid stellar models, leading to more energetic explosions (magenta line in Figure 4).

The structure of such hybrid proto-WDs is susceptible to mixing due to their composition gradient. As Brooks et al. (2017) point out, the ONe mantle has been processed by a carbon burning front that involves several weak reactions, resulting in a lower electron-to-baryon fraction (Y_e) with respect to the CO core. This configuration is stable against convection as long as the ONe ashes in the top, heavy fluid (mantle) are much hotter than the CO bottom, light fluid (core). As the temperature gradient is reduced, the core-mantle interface will be subjected to thermocompositional convection and destroyed in a timescale of the order of Kyr, as the WD moves toward an isothermal profile. By the time an explosion can occur, the WD should be well mixed. The same process can re-distribute the residual carbon within ONe cores and reduce it to such levels so a thermal runaway would be unlikely making the AIC a more plausible scenario.

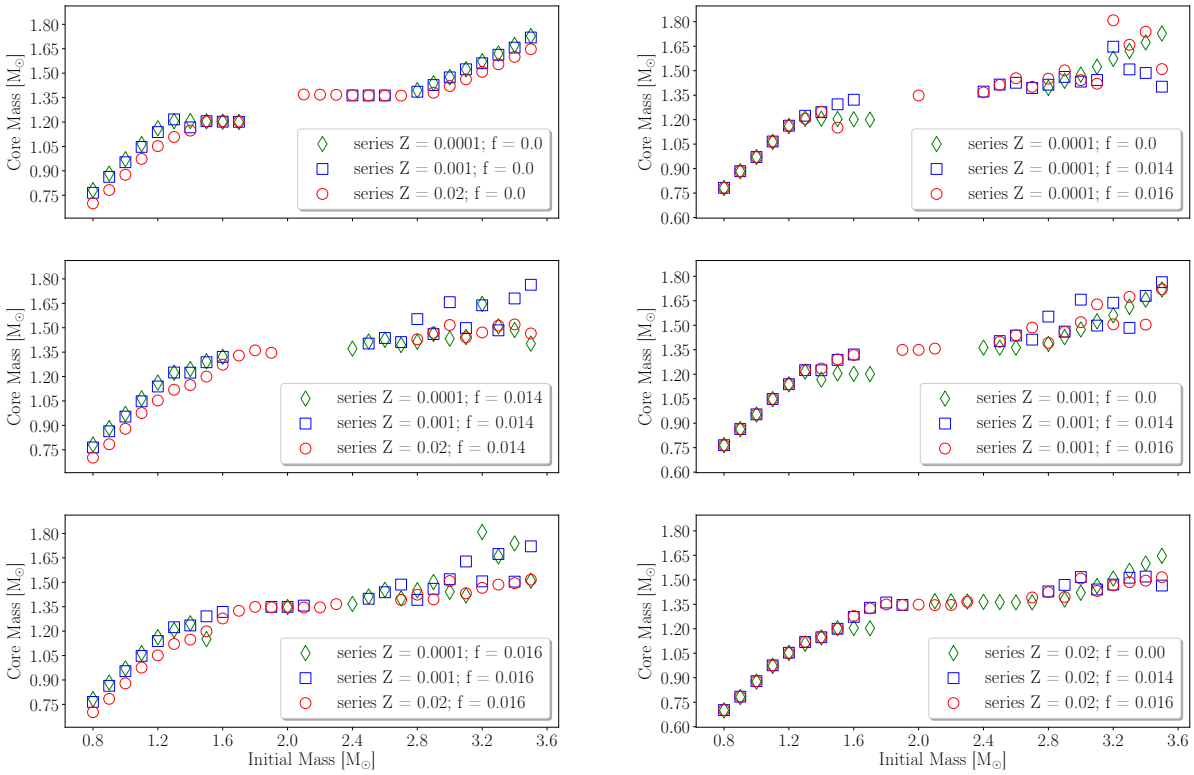

Figure 2. Core growth for different metallicity environments (left), and overshooting factors (right). Models that experience thermal runaway develop a core of $M_c \sim 1.36 \pm 0.01$ $M_\odot$ (plateau) due to He-shell burning. Missing data points correspond to models which their evolution ended abruptly, hence their final core mass could not be estimated.

3.5. *Observational Consequences*

[Antoniadis]

4. DISCUSSION AND FUTURE WORK

5. ACKNOWLEDGEMENTS

Software: MESA[3] (Paxton et al. 2011, 2013, 2015, 2018, 2019), ASTROPY[4] (Astropy Collaboration et al. 2013, 2018), MESAPLOT[5] (Farmer 2018), MESAREADER[6]

[3] http://mesastar.org
[4] http://www.astropy.org
[5] https://github.com/rjfarmer/mesaplot
[6] http://wmwolf.github.io/MESA_Reader

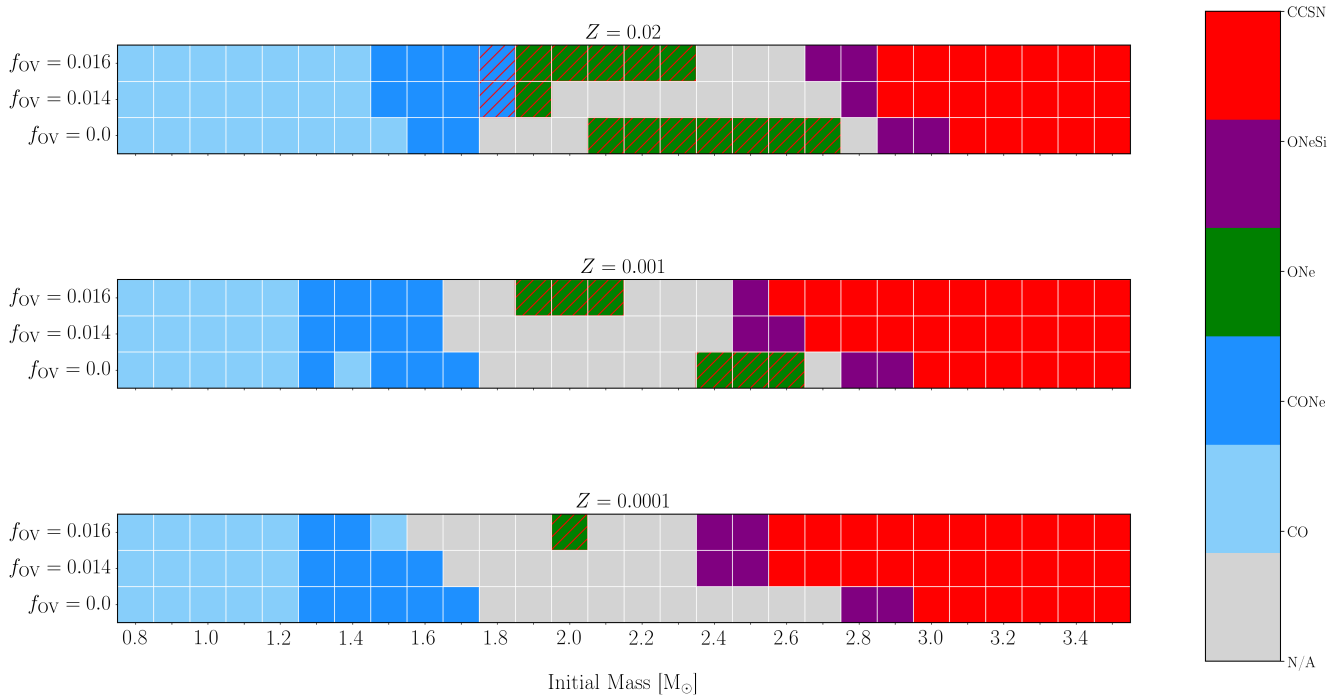

Figure 3. Full parameter space in raster format. Metallicity for the bottom, middle, and top panel is $Z = 0.0001$, $Z = 0.001$, and $Z = 0.02$ respectively, whilst the color-bar indicates the composition of the model at the moment our simulation was terminated. Hatched regions show models that have developed a core mass in the range 1.35 - 1.37 $M_\odot$, and can experience a thermonuclear runaway.

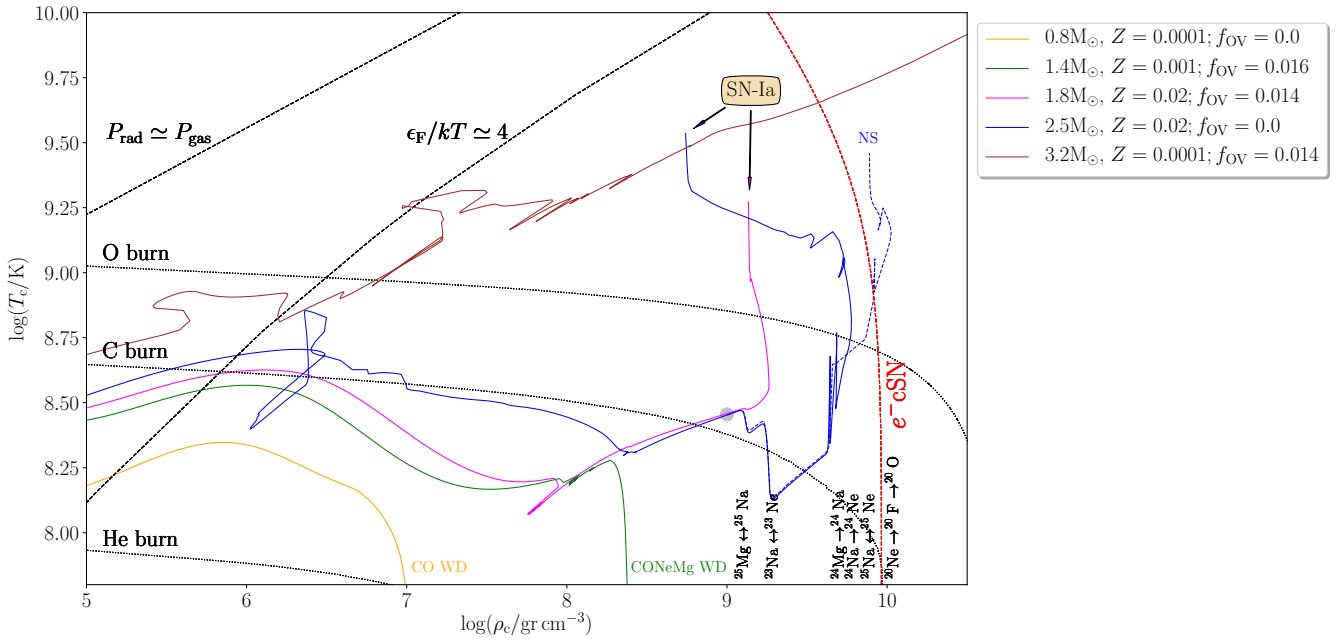

Figure 4. Examples of the evolution of different initial masses in the $\log(\rho_c) - \log(T_c)$ plane. Black dotted lines show approximate ignition curves taken from MESA. Black dashed lines indicate different pressure regimes whilst the red dashed curve shows the approximate threshold for e-captures on ^{20}Ne nuclei. The blue dashed line refers to the same stellar model as the one with the solid blue line; the only difference is that for the former, all carbon-participating reaction have been switched off leading most likely to an ECSN.

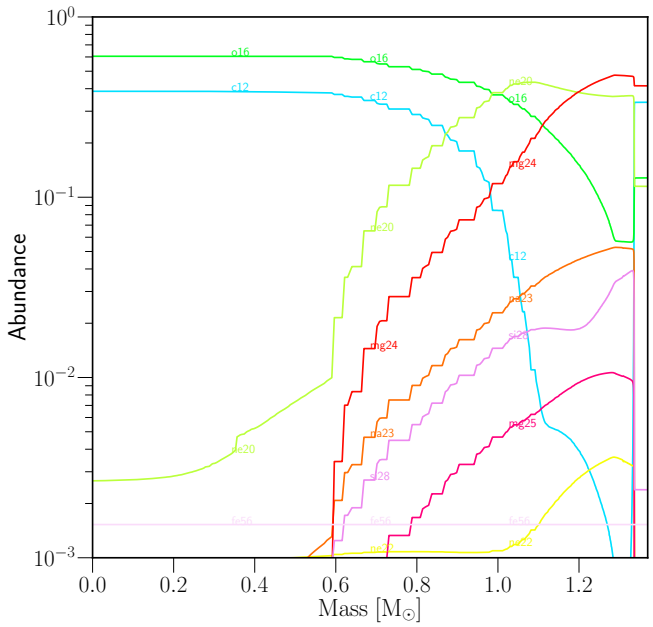

(a) Structure of the $1.8M_{\odot}$, $Z = 0.02$; $f_{OV} = 0.014$ stellar model, when $\log(\rho_c) = 9.0$ (indicated by the grey circle in Figure 4).

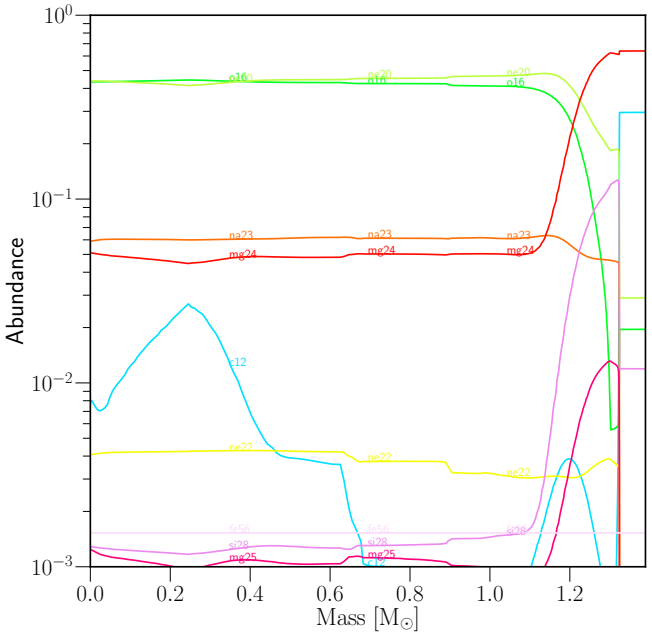

(b) Structure of the $2.5M_{\odot}$, $Z = 0.02$; $f_{OV} = 0.0$ stellar model, when $\log(\rho_c) = 9.0$ (indicated by the grey circle in Figure 4). Residual carbon from previous burning stages is visible.

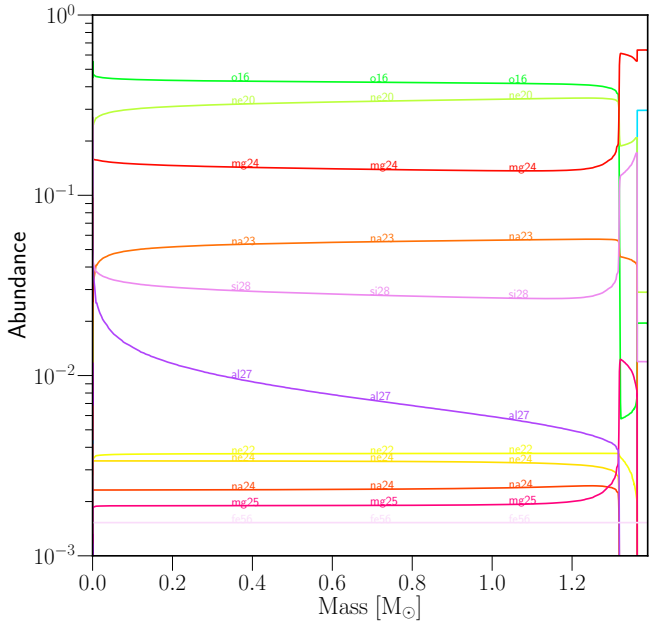

(c) Final structure of the $2.5M_{\odot}$ stellar model. Residual carbon leads to TNE.

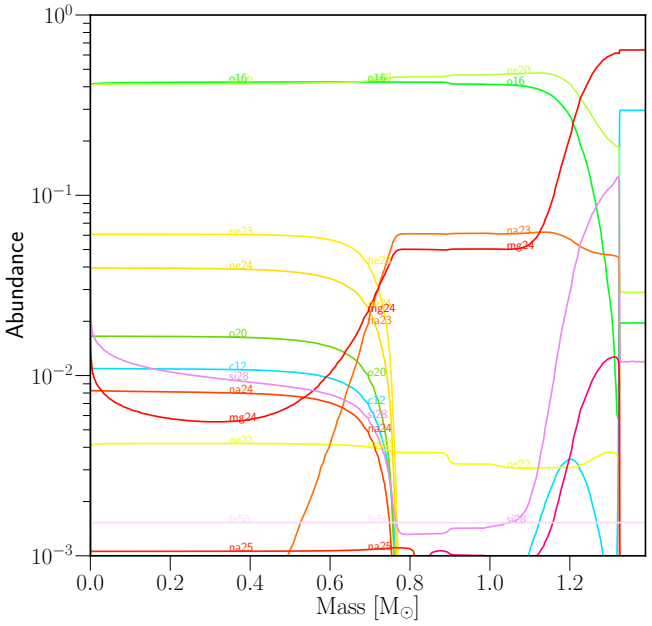

(d) Final structure of the $2.5M_{\odot}$ stellar model, in the case where carbon consuming nuclear reactions have been turned-off. The core reach density for Urca process on Ne nuclei to commence, leading to formation of ^{20}O, and ultimately to ECSN.

Figure 5. Abundance profiles of our fiducial models during various evolutionary stages.

REFERENCES

Astropy Collaboration, Robitaille, T. P., Tollerud, E. J., et al. 2013, A&A, 558, A33

Astropy Collaboration, Price-Whelan, A. M., Sipőcz, B. M., et al. 2018, The Astronomical Journal, 156, 123

Barkat, Z., & Wheeler, J. C. 1990, ApJ, 355, 602

Brooks, J., Schwab, J., Bildsten, L., Quataert, E., & Paxton, B. 2017, The Astrophysical Journal, 843, 151

Brooks, J., Schwab, J., Bildsten, L., Quataert, E., & Paxton, B. 2017, ApJL, 834, L9

Brown, J. M., Garaud, P., & Stellmach, S. 2013, The Astrophysical Journal, 768, 34

Bruenn, S. W. 1973, ApJL, 183, L125

Chen, M. C., Herwig, F., Denissenkov, P. A., & Paxton, B. 2014, MNRAS, 440, 1274

de Jager, C., Nieuwenhuijzen, H., & van der Hucht, K. A. 1988, Astronomy and Astrophysics Supplement Series, 72, 259

Denissenkov, P. A., Herwig, F., Truran, J. W., & Paxton, B. 2013, The Astrophysical Journal, 772, 37

Denissenkov, P. A., Truran, J. W., Herwig, F., et al. 2015, MNRAS, 447, 2696

Farmer, R. 2018, rjfarmer/mesaplot

Farmer, R., Fields, C. E., & Timmes, F. X. 2015, The Astrophysical Journal, 807, 184

Fischer, T., Whitehouse, S. C., Mezzacappa, A., Thielemann, F. K., & Liebendörfer, M. 2010, A&A, 517, A80

Gamow, G., & Schoenberg, M. 1941, Phys. Rev., 59, 539

Glebbeek, E., Gaburov, E., de Mink, S. E., Pols, O. R., & Portegies Zwart, S. F. 2009, Astronomy and Astrophysics, 497, 255

Gutiérrez, J., Canal, R., & García-Berro, E. 2005, A&A, 435, 231

Henyey, L., Vardya, M. S., & Bodenheimer, P. 1965, The Astrophysical Journal, 142, 841

Herwig, F. 2000, Astronomy and Astrophysics, 360, 952

Hillebrandt, W., & Niemeyer, J. C. 2000, Annual Review of Astronomy and Astrophysics, 38, 191

Iglesias, C. A., & Rogers, F. J. 1996, The Astrophysical Journal, 464, 943

Itoh, N., Tomizawa, N., Tamamura, M., Wanajo, S., & Nozawa, S. 2002, The Astrophysical Journal, 579, 380

Jones, S., Röpke, F. K., Pakmor, R., et al. 2016, A&A, 593, A72

Jones, S., Hirschi, R., Nomoto, K., et al. 2013, The Astrophysical Journal, 772, 150

Kippenhahn, R., Ruschenplatt, G., & Thomas, H.-C. 1980, Astronomy and Astrophysics, 91, 175

Knigge, C., Coe, M. J., & Podsiadlowski, P. 2011, Nature, 479, 372

Langer, N. 1991, Astronomy and Astrophysics, 252, 669

Langer, N., Fricke, K. J., & Sugimoto, D. 1983, Astronomy and Astrophysics, 126, 207

Lecoanet, D., Schwab, J., Quataert, E., et al. 2016, ApJ, 832, 71

Lesaffre, P., Podsiadlowski, P., & Tout, C. A. 2005, MNRAS, 356, 131

Livio, M., & Mazzali, P. 2018, PhR, 736, 1

Moriya, T. J., Tominaga, N., Langer, N., et al. 2014, A&A, 569, A57

Nomoto, K. 1984, ApJ, 277, 791

Nomoto, K., & Kondo, Y. 1991, ApJL, 367, L19

Nugis, T., & Lamers, H. J. G. L. M. 2000, Astronomy and Astrophysics, 360, 227

Paczyński, B. 1972, Astrophys. Lett., 11, 53

—. 1973, Astrophys. Lett., 15, 147

Paxton, B., Bildsten, L., Dotter, A., et al. 2011, The Astrophysical Journal Supplement Series, 192, 3

Paxton, B., Cantiello, M., Arras, P., et al. 2013, The Astrophysical Journal Supplement Series, 208, 4

Paxton, B., Marchant, P., Schwab, J., et al. 2015, The Astrophysical Journal Supplement Series, 220, 15

Paxton, B., Schwab, J., Bauer, E. B., et al. 2018, The Astrophysical Journal Supplement Series, 234, 34

Paxton, B., Smolec, R., Gautschy, A., et al. 2019, arXiv e-prints, arXiv:1903.01426

Potekhin, A. Y., Chabrier, G., & Rogers, F. J. 2009, Phys. Rev. E, 79, 016411

Schwab, J., Bildsten, L., & Quataert, E. 2017, MNRAS, 472, 3390

Schwab, J., & Garaud, P. 2019, ApJ, 876, 10

Schwab, J., Quataert, E., & Bildsten, L. 2015, Monthly Notices of the Royal Astronomical Society, 453, 1910

Schwab, J., & Rocha, K. A. 2019, The Astrophysical Journal, 872, 131

Siess, L. 2006, A&A, 448, 717

—. 2009, A&A, 497, 463

Stein, J., Barkat, Z., & Wheeler, J. C. 1999, ApJ, 523, 381

Suzuki, T., Toki, H., & Nomoto, K. 2016, The Astrophysical Journal, 817, 163

Tauris, T. M., Langer, N., Moriya, T. J., et al. 2013, ApJ, 778, L23

Tauris, T. M., Langer, N., & Podsiadlowski, P. 2015, MNRAS, 451, 2123

Timmes, F. X., Woosley, S. E., & Taam, R. E. 1994, ApJ, 420, 348

Tsuruta, S., & Cameron, A. 1970, Astrophysics and Space Science, 7, 374

Waldman, R., & Barkat, Z. 2007, The Astrophysical Journal, 665, 1235

Wang, B. 2018, Research in Astronomy and Astrophysics, 18, 049

Wang, B., & Han, Z. 2012, New Astronomy Reviews, 56, 122

Woosley, S. E., Wunsch, S., & Kuhlen, M. 2004, ApJ, 607, 921

Zha, S., Leung, S.-C., Suzuki, T., & Nomoto, K. 2019, arXiv e-prints, arXiv:1907.04184

Chapter 4

DISCUSSION

BIBLIOGRAPHY

Abbott, B. P., Abbott, R., Abbott, T. D., et al. 2017, Phys. Rev. Lett., 119, 161101

Branch, D. & Wheeler, J. C. 2017, Supernova Explosions (Springer)

Cantiello, M. & Langer, N. 2010, Astronomy and Astrophysics, 521, A9

Celletti, A. & Giorgilli, A. 1990, Celestial Mechanics and Dynamical Astronomy, 50, 31

Charbonnel, C. & Zahn, J.P. 2007, Astronomy and Astrophysics, 467, L15

Chiosi, C. & Maeder, A. 1986, Annual Review of Astronomy and Astrophysics, 24, 329

Clayton, D. 1968, Principles of Stellar Evolution and Nucleosynthesis (McGraw-Hill)

Couch, S. M. 2017, 375

de Jager, C., Nieuwenhuijzen, H., & van der Hucht, K. A. 1988, Astronomy and Astrophysics Supplement Series, 72, 259

Dewi, J. D. M. & Pols, O. R. 2003, Monthly Notice of the Royal Astronomical Society, 344, 629

Eggleton, P. 2006, Evolutionary Processes in Binary and Multiple Stars (Cambridge University Press)

Eggleton, P. P. 1983, The Astrophysical Journal, 268, 368

Filippenko, A. V. 1997, Annual Review of Astronomy and Astrophysics, 35, 309

Giacobbo, N. & Mapelli, M. 2018, Monthly Notices of the Royal Astronomical Society [[arXiv]1805.11100]

Gilmer, M. S., Kozyreva, A., Hirschi, R., Fröhlich, C., & Yusof, N. 2017, The Astrophysical Journal, 846, 100

Glebbeek, E., Gaburov, E., de Mink, S. E., Pols, O. R., & Portegies Zwart, S. F. 2009, Astronomy and Astrophysics, 497, 255

Habets, G. 1986a, Astronomy and Astrophysics, 165, 95

Habets, G. 1986b, Astronomy and Astrophysics, 167, 61

Hamann, W. R., Koesterke, L., & Wessolowski, U. 1995, Astronomy and Astrophysics, 299, 151

Hamann, W.-R., Schoenberner, D., & Heber, U. 1982, Astronomy and Astrophysics, 116, 273

Han, Z., Podsiadlowski, P., Maxted, P. F. L., & Marsh, T. R. 2003, Monthly Notices of the Royal Astronomical Society, 341, 669

Han, Z., Podsiadlowski, P., Maxted, P. F. L., Marsh, T. R., & Ivanova, N. 2002, Monthly Notices of the Royal Astronomical Society, 336, 449

Heber, U. 2009, Annual Review of Astronomy and Astrophysics, 47, 211

Heger, A., Langer, N., & Woosley, S. E. 2000, The Astrophysical Journal, 528, 368

Heger, A., Woosley, S. E., & Spruit, H. C. 2005, The Astrophysical Journal, 626, 350

Henyey, L., Vardya, M. S., & Bodenheimer, P. 1965, The Astrophysical Journal, 142, 841

Herwig, F. 2000, Astronomy and Astrophysics, 360, 952

Hillebrandt, W. & Niemeyer, J. C. 2000, Annual Review of Astronomy and Astrophysics, 38, 191

Hirschi, R., Meyne, G., & Maeder, A. 2004, Astronomy and Astrophysics, 425, 649

Iglesias, C. A. & Rogers, F. J. 1996, The Astrophysical Journal, 464, 943

Itoh, N., Tomizawa, N., Tamamura, M., Wanajo, S., & Nozawa, S. 2002, The Astrophysical Journal, 579, 380

Ivanova, N. 2015, Binary Evolution: Roche Lobe Overflow and Blue Stragglers, ed. H. M. J. Boffin, G. Carraro, & G. Beccari, 179

Ivanova, N., Belczynski, K., Kalogera, V., Rasio, F. A., & Taam, R. E. 2003, The Astrophysical Journal, 592, 475

Ivanova, N., Justham, S., Chen, X., et al. 2013, The Astronomy and Astrophysics Review, 21, 59

Ivanova, N. & Taam, R. E. 2003, The Astrophysical Journal, 599, 516

Izzard, R. G., Hall, P. D., Tauris, T. M., & Tout, C. A. 2012, in IAU Symposium, Vol. 283, IAU Symposium, 95–102

Jones, S., Röpke, F. K., Pakmor, R., et al. 2016, Astronomy and Astrophysics, 593, A72

Kalogera, V. & Webbink, R. F. 1996, The Astrophysical Journal, 458, 301

Kippenhahn, R., Ruschenplatt, G., & Thomas, H.-C. 1980, Astronomy and Astrophysics, 91, 175

Kippenhahn, R. & Weigert, A. 1967, Zeitschrift für Astrophysik, 65, 251

Kippenhahn, R., Weigert, A., & Weiss, A. 2012, Stellar Structure and Evolution, 2nd edn. (Springer)

Kozyreva, A., Gilmer, M., Hirschi, R., et al. 2017, Monthly Notices of the Royal Astronomical Society, 464, 2854

Lamers, H. & Cassinelli, J. 1999, Introduction to Stellar Winds (Cambridge University Press)

Langer, N. 1989, Astronomy and Astrophysics, 220, 135

Langer, N. 1991, Astronomy and Astrophysics, 252, 669

Langer, N. 2012, Annual Review of Astronomy and Astrophysics, 50, 107

Langer, N., Fricke, K. J., & Sugimoto, D. 1983, Astronomy and Astrophysics, 126, 207

Langer, N., Heger, A., & Fliegner, J. 1997, in IAU Symposium, Vol. 189, IAU Symposium, ed. T. R. Bedding, A. J. Booth, & J. Davis, 343–348

Langer, N., Norman, C. A., de Koter, A., et al. 2007, Astronomy and Astrophysics, 475, L19

Lauterborn, D. 1970, Astronomy and Astrophysics, 7, 150

Maeder, A. 1987, Astronomy and Astrophysics, 178, 159

Maeder, A., Meynet, G., Hirschi, R., & Ekström, S. 2006, Rotational Mixing in Massive Stars and Its Many Consequences, ed. S. Randich & L. Pasquini, 308

Moriya, T. J., Mazzali, P. A., Tominaga, N., et al. 2017, Monthly Notices of the Royal Astronomical Society, 466, 2085

Müller, B., Heger, A., Liptai, D., & Cameron, J. B. 2016, Monthly Notices of the Royal Astronomical Society, 460, 742

Nomoto, K. 1984, The Astrophysical Journal, 277, 791

Nomoto, K. 1987, The Astrophysical Journal, 322, 206

Nomoto, K., Tominaga, N., & Blinnikov, S. I. 2014, in American Institute of Physics Conference Series, Vol. 1594, American Institute of Physics Conference Series, ed. S. Jeong, N. Imai, H. Miyatake, & T. Kajino, 258–265

Nugis, T. & Lamers, H. J. G. L. M. 2000, Astronomy and Astrophysics, 360, 227

Palacios, A. 2013, in EAS Publications Series, Vol. 62, EAS Publications Series, ed. P. Hennebelle & C. Charbonnel, 227–287

Paxton, B., Bildsten, L., Dotter, A., et al. 2011, The Astrophysical Journal Supplement Series, 192, 3

Paxton, B., Cantiello, M., Arras, P., et al. 2013, The Astrophysical Journal Supplement Series, 208, 4

Paxton, B., Marchant, P., Schwab, J., et al. 2015, The Astrophysical Journal Supplement Series, 220, 15

Paxton, B., Schwab, J., Bauer, E. B., et al. 2018, The Astrophysical Journal Supplement Series, 234, 34

Peters, P. C. 1964, Phys. Rev., 136, B1224

Podsiadlowski, P. 2014, The evolution of binary systems, ed. I. González Martínez-País, T. Shahbaz, & J. Casares Velázquez, Canary Islands Winter School of Astrophysics (Cambridge University Press), 45–88

Poelarends, A. J. T., Wurtz, S., Tarka, J., Cole Adams, L., & Hills, S. T. 2017, The Astrophysical Journal, 850, 197

Postnov, K. A. & Yungelson, L. R. 2014, Living Reviews in Relativity, 17, 3

Potekhin, A. Y., Chabrier, G., & Rogers, F. J. 2009, Phys. Rev. E, 79, 016411

Prialnik, D. 2000, An Introduction to the Theory of Stellar Structure and Evolution (Cambridge University Press)

Rappaport, S., Verbunt, F., & Joss, P. C. 1983, The Astrophysical Journal, 275, 713

Riles, K. 2013, Progress in Particle and Nuclear Physics, 68, 1

Roxburgh, I. W. 1998, in Astronomical Society of the Pacific Conference Series, Vol. 138, 1997 Pacific Rim Conference on Stellar Astrophysics, ed. K. L. Chan, K. S. Cheng, & H. P. Singh, 411

Saslaw, W. C. & Schwarzschild, M. 1965, The Astrophysical Journal, 142, 1468

Schwarz, R., Bazso, A., Erdi, B., & Funk, B. 2012, Monthly Notices of the Royal Astronomical Society, 427, 397

Siess, L. & Lebreuilly, U. 2018, Astronomy and Astrophysics, 614, A99

Smartt, S. J. 2009, Annual Review of Astronomy and Astrophysics, 47, 63

Smith, N. 2014, Annual Review of Astronomy and Astrophysics, 52, 487

Soberman, G. E., Phinney, E. S., & van den Heuvel, E. P. J. 1997, Astronomy and Astrophysics, 327, 620

Spruit, H. 2013, Astronomy and Astrophysics, 552, A76

Spruit, H. C. 2002, Astronomy and Astrophysics, 381, 923

Stothers, R. B. & Chin, C.-W. 1990, The Astrophysical Journal, 348, L21

Sweigart, A. V. 1997, The Astrophysical Journal, 427, L23

Szebehely, V. 1967, Theory of Orbits: The Restricted Problem of Three Bodies (Academic Press, New York and London)

Tauris, T. M., Kramer, M., Freire, P. C. C., et al. 2017, The Astrophysical Journal, 846, 170

Tauris, T. M., Langer, N., Moriya, T. J., et al. 2013, The Astrophysical Journal Letters, 778, L23

Tauris, T. M., Langer, N., & Podsiadlowski, P. 2015, Monthly Notices of the Royal Astronomical Society, 451, 2123

Tauris, T. M. & van den Heuvel, E. P. J. 2006, in Compact stellar X-ray sources, ed. W. H. G. Lewin & M. van der Klis, 623–665

Turatto, M. 2003, in Lecture Notes in Physics, Berlin Springer Verlag, Vol. 598, Supernovae and Gamma-Ray Bursters, ed. K. Weiler, 21–36

van der Sluijs, M. V. 2006, PhD thesis, Universiteit Utrecht

Wang, B. 2018, Research in Astronomy and Astrophysics, 18, 049

Weigert, A. 1968, Mitteilungen der Astronomischen Gesellschaft Hamburg, 25, 19

Wilson, R. E. 1981, Astronomy and Astrophysics, 99, 43

Woosley, S. E. 2017, The Astrophysical Journal, 836, 244

Yakut, K., Kalomeni, B., & Tout, C. A. 2008, ArXiv e-prints [[arXiv]0811.0455]

Yoon, S.-C. 2017, Monthly Notices of the Royal Astronomical Society, 470, 3970

Yoon, S.-C. & Langer, N. 2005, Astronomy and Astrophysics, 443, 643

Yoon, S.-C., Woosley, S. E., & Langer, N. 2010, The Astrophysical Journal, 725, 940

Zingale, M. 2016, equipotentials.py, https://github.com/zingale/astro_animations/blob/master/binary_exoplanets/equipotentials/equipotentials.py